



Imaging findings during and after percutaneous cryoablation of hepatic tumors

Lisa Ratanaprasatporn¹ · Nisha Sainani¹ · Jeremy B. Duda¹ · Ayaz Aghayev¹ · Servet Tatli¹ · Stuart G. Silverman¹ · Paul B. Shyn¹

Published online: 19 April 2019
© Springer Science+Business Media, LLC, part of Springer Nature 2019

Abstract

Objective Imaging plays a key role in the assessment of patients before, during, and after percutaneous cryoablation of hepatic tumors. Intra-procedural and early post-procedure imaging with CT and MRI is vital to the assessment of technical success including adequacy of ablation zone coverage. Recognition of the normal expected post-procedure findings of hepatic cryoablation such as ice ball formation, hydrodissection, and the normal appearance of the ablation zone is crucial to be able to differentiate from complications including vascular, biliary, or non-target organ injury. Delayed imaging is essential for determination of clinical effectiveness and detection of unexpected findings such as residual unablated tumor and local tumor progression. The purpose of this article is to review the spectrum of expected and unexpected imaging findings that may occur during or after percutaneous cryoablation of hepatic tumors.

Conclusion Differentiating expected from unexpected findings during and after hepatic cryoablation helps radiologists identify residual or recurrent tumor and detect procedure-related complications.

Keywords Hepatic · Cryoablation · Ice-ball · Percutaneous · CT · MRI

Introduction

Image-guided percutaneous cryoablation is an effective, minimally-invasive treatment option for patients with selected primary or secondary hepatic malignancies [1, 2]. Pioneered as an alternative to surgical resection that often necessitated partial hepatectomy, cryoablation was first used to treat hepatic tumors during open surgery guided with intraoperative ultrasound (US) so that unresectable tumors could be treated and more liver tissue preserved [3–5]. However, cryosurgery required large cryoprobes measuring up to 9 mm in diameter; freezing times averaged 30 min, procedure times occasionally lasted up to 5 h, and complications such as liver capsule cracking, bleeding, and even ‘cryo-shock’ were observed [3–7]. The development of thinner, more efficient cryoprobes led to the development of percutaneous approaches under US, computed tomography (CT),

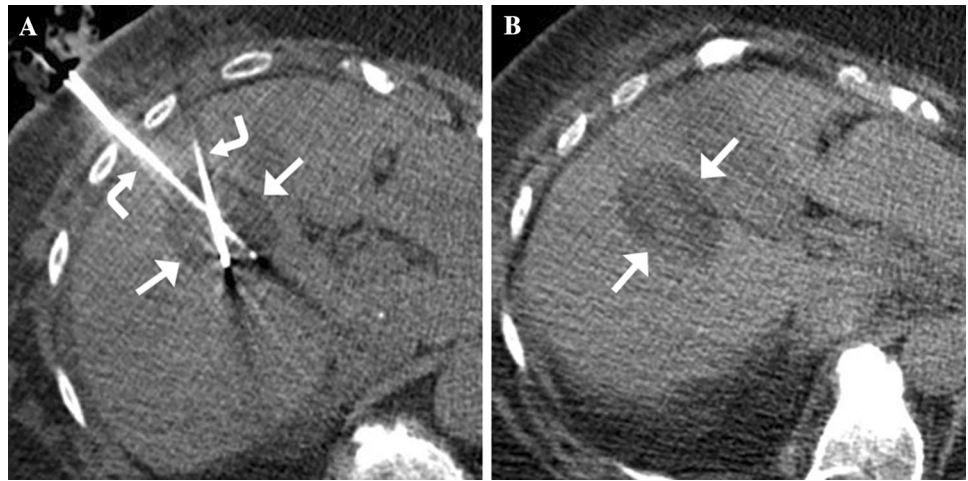
and magnetic resonance imaging (MRI) guidance [8–10]. Since then, percutaneous, image-guided hepatic cryoablation has been shown to be an effective treatment option for patients with selected primary or secondary hepatic malignancies [11, 12]. Unlike US in which only the echo-reflective near edge of the ice ball is seen, CT and MRI both allow visualization of the entire ice ball [13]. In addition to the less invasive nature of a percutaneous approach, it is thought that the physiologic compressive tamponade effect of the abdominal wall upon the liver (preventing deformation of the hepatic ice ball) and the lack of exposure of the iceball to air help prevent capsule cracking [9, 14, 15].

Early post-procedure imaging, generally the day of the cryoablation procedure or the next day may be used to evaluate both the technical success and to identify early complications. Delayed imaging is used routinely to assess the clinical effectiveness of the ablation and to identify delayed complications. Ablations cause imaging findings which are ‘expected’ i.e., a normal result of the procedure, and ‘unexpected’, i.e., indicating the presence of a complication or an unsuccessful procedure. Differentiating expected from unexpected findings is important in order to diagnose residual unablated tumor, local tumor progression, and

✉ Nisha Sainani
drnisainani@gmail.com

¹ Division of Abdominal Imaging and Intervention,
Department of Radiology, Brigham and Women’s Hospital,
75 Francis Street, Boston, MA 02115, USA

Fig. 1 Eighty-two-year-old female who underwent CT-guided cryoablation of a breast cancer metastasis. **a** Axial, intra-procedural, unenhanced CT image obtained during cryoablation reveals two cryoprobes (curved arrows) in the right hepatic lobe within the target mass and surrounded by the sharply-margined hypoattenuating ice ball (straight arrows). **b** Axial, unenhanced CT image obtained immediately after cryoablation reveals the ovoid hypoattenuating ice ball (arrows) which is just beginning to thaw



complications. The purpose of this article is to review the spectrum of expected and unexpected imaging findings that may occur during or after percutaneous cryoablation of hepatic tumors.

Imaging modalities

Imaging of the liver is obtained before, during and after the ablation procedure. MRI is the preferred modality at our institution for pre- and post-procedure imaging. Baseline pre-procedure MRI is obtained no more than 1 month prior to the ablation to allow treatment planning. Cryoablation is performed under CT or MRI guidance [16]. Post-procedure MRI is performed within 24 h to assess ablation zone coverage of the tumor, to evaluate potential complications, and to provide a baseline for follow-up.

Subsequently, MRI is performed at 3, 6, 9, and 12 months followed by yearly imaging.

The MRI protocol utilizes axial and coronal single-shot fast spin echo (ssFSE/HASTE) T2-weighted sequences without fat saturation (TR/TE, 1000/180; slice thickness, 6 mm; interslice gap, 1.2 mm; matrix size, 256 × 256), axial fast spin echo (FSE) T2-weighted sequences with fat saturation (TR/TE, 4700/85; slice thickness, 6 mm; interslice gap, 1.2 mm; matrix size, 320 × 320; receive bandwidth, 32 kHz), and an unenhanced axial 3D gradient-breadth hold examination (VIBE) T1-weighted sequence with fat saturation (TR/TE, 3.3/1.6; slice thickness, 4 mm; matrix size, 266 × 164; receive bandwidth, 64 kHz; flip angle, 15°). These sequences are followed by IV injection of gadolinium-based contrast agent (0.1 mmol/kg of body weight) and acquisition of axial 3D gradient-recalled echo (VIBE) T1-weighted fat-saturation sequences at three

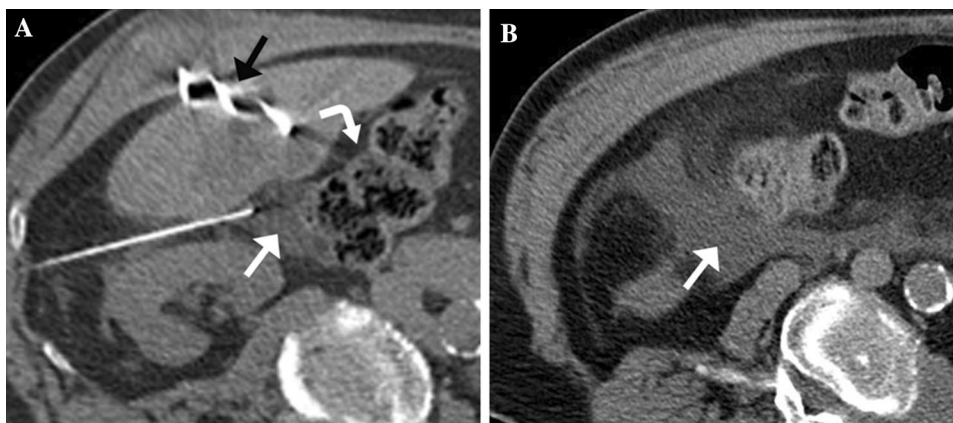
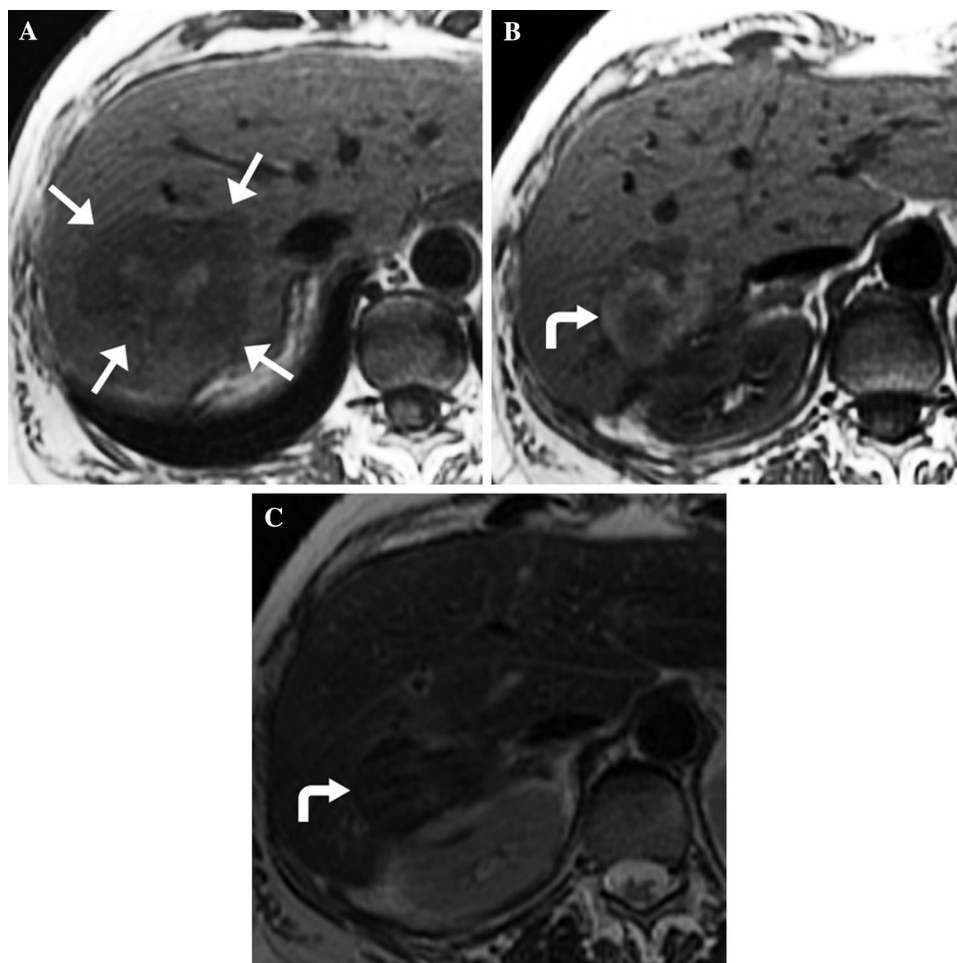


Fig. 2 Eighty-one-year-old male who underwent CT-guided cryoablation of an esophageal cancer metastasis. **a** Axial, intra-procedural, unenhanced CT image reveals cryoprobes with motion artifacts (black arrow) in the target mass in the right hepatic lobe. Saline was instilled through a 20G needle for hydrodissection (white arrow) to

displace the colon (curved arrow) from the ablation zone. **b** Immediate post-procedure CT demonstrates artificial ascites (arrow) in the right lower quadrant of the abdomen which was instilled for hydrodissection

Fig. 3 Fifty-four-year-old female who underwent cryoablation of a colon cancer metastasis. **a** Axial, T1-weighted, 24-h post-procedure MR image demonstrates a T1 hypointense ablation zone (straight arrows) surrounding the ablated mass with T1 hyperintense areas within indicating coagulative necrosis. **b** and **c** Axial, T1-weighted, 24-h, post-procedure (**b**) and T2-weighted (**c**) MR images demonstrate T1 hyperintense and T2 hypointense changes which are probably due to desiccated tissue at the inferior aspect of the ablation zone (curved arrows) rather than a hematoma, an expected finding



consecutive 30-s intervals followed by a delayed acquisition at 5 min.

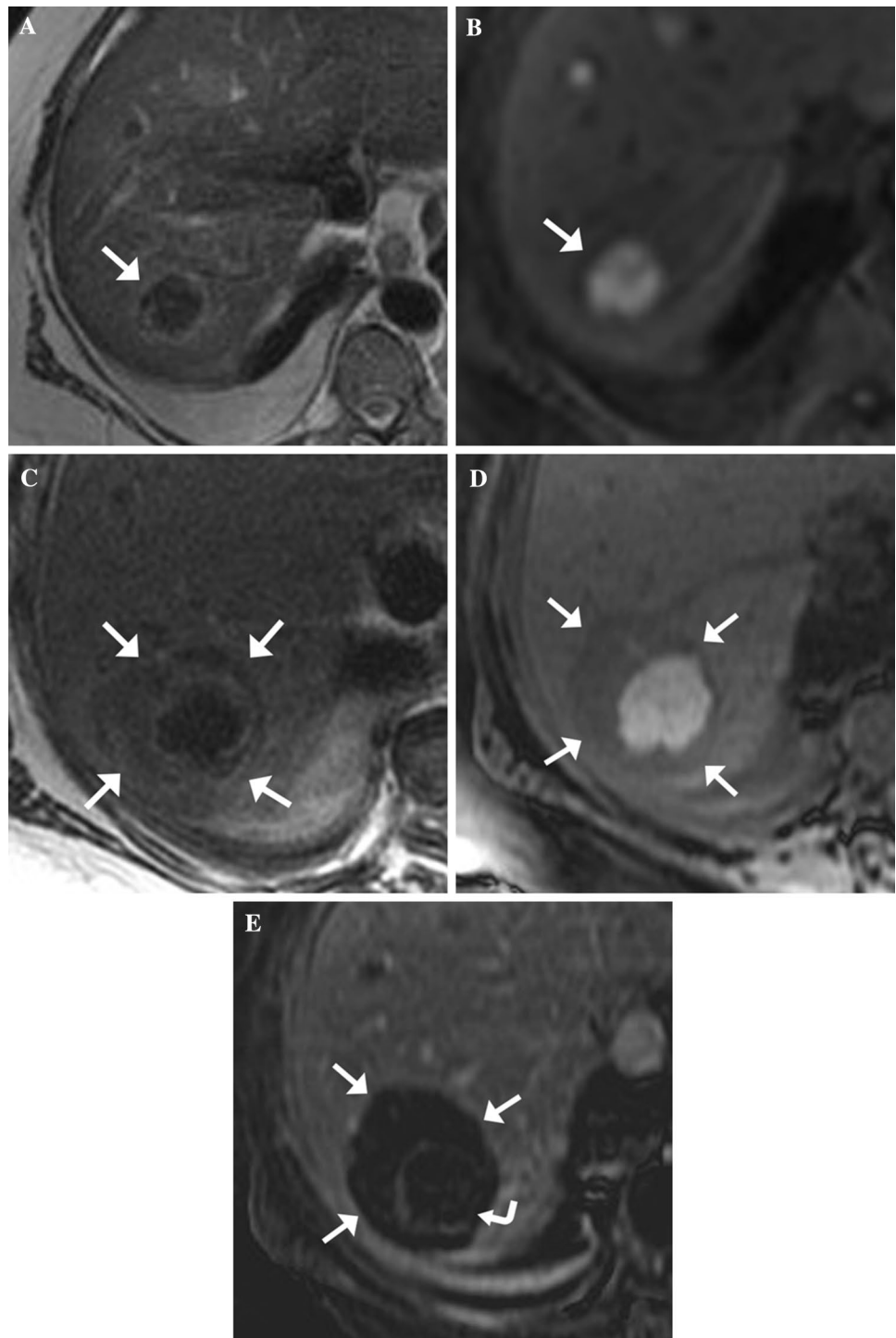
Diffusion-weighted imaging (DWI) is not routinely included in our imaging protocol. In our experience, we have found DWI signal to be quite variable in the ablation zone making adequate interpretation of this imaging technique challenging. In a study by Weiss et al. [17] which evaluated the diagnostic accuracy of individual sequences of a clinical routine liver MRI protocol for the detection of local tumor progression after radiofrequency ablation of hepatic malignancies, DWI demonstrated the highest discrepancy between readers when compared to unenhanced T1-FLASH 2D and contrast-enhanced T1-VIBE sequences. This was felt to be due to poor image quality due to low signal intensity. Because DWI is sensitive to alterations in tissue microenvironment that result from ablation, diffusion restriction in the ablation zone does not necessarily indicate a malignant process. In fact, a common finding in DWI immediately after radiofrequency ablation is a hyperintense rim in the periphery of the

ablation zone which should not be mistaken for residual tumor [18].

In patients with a contraindication to MRI or gadolinium-based contrast agents, multiphase contrast-enhanced CT is performed. The CT protocol begins with unenhanced 5-mm-thick images acquired through the upper abdomen. Non-ionic iodinated contrast material (300 or 350 mg I/mL; 100–150 mL depending on patient weight) is injected intravenously through a power injector at a rate of 4–5 mL/s; 40 s after contrast material injection, 3-mm-thick arterial-dominant phase images are acquired cranio-caudal through the upper abdomen including the liver in case of hypervascular tumors; 70 s after contrast injection, 5-mm-thick portal venous phase images are acquired cranio-caudal from the diaphragm to the pubic symphysis.

CT perfusion imaging (CT-PI) is a bolus-tracking technique performed on multi-detector CT scanners which has been shown to be useful in the detection of cancers as well as efficacy of transcatheter arterial chemoembolization (TACE) and radiofrequency ablation of hepatic tumors [19]. Several

Fig. 4 Fifty-four-year-old female who underwent cryoablation of a melanoma metastasis. **a** and **b** Axial, pre-procedure, T2-weighted (**a**) and diffusion-weighted (**b**) MR images show a T2 hypointense and diffusion restricting (arrows) melanoma metastasis in the right hepatic lobe. **c** and **d** Axial, 24-h, post-procedure, T2-weighted (**c**) and T1-weighted (**d**) MR images show a mildly T2 hypointense and T1 hypointense ablation zone (arrows) engulfing the mass which is T2 hypointense and T1 hyperintense with satisfactory margins. **e** Axial, post-contrast, T1-weighted, subtraction image demonstrates no enhancement of the mass, except mild rim enhancement (curved arrow), and non-enhancing ablation zone (arrows)



studies have demonstrated a correlation between histologic biomarkers of angiogenesis in several tumors including pancreatic and colorectal tumors and tumor perfusion parameters such as regional blood flow, blood volume, and permeability of tumor vessels [20–22]. However, we do not use CT perfusion imaging in our practice due to current work flow limitations.

Mechanism of cryoablation

The various imaging findings in the post-cryoablation patient are attributable to its unique mechanism of cell death, and are distinct from the appearance after heat-based

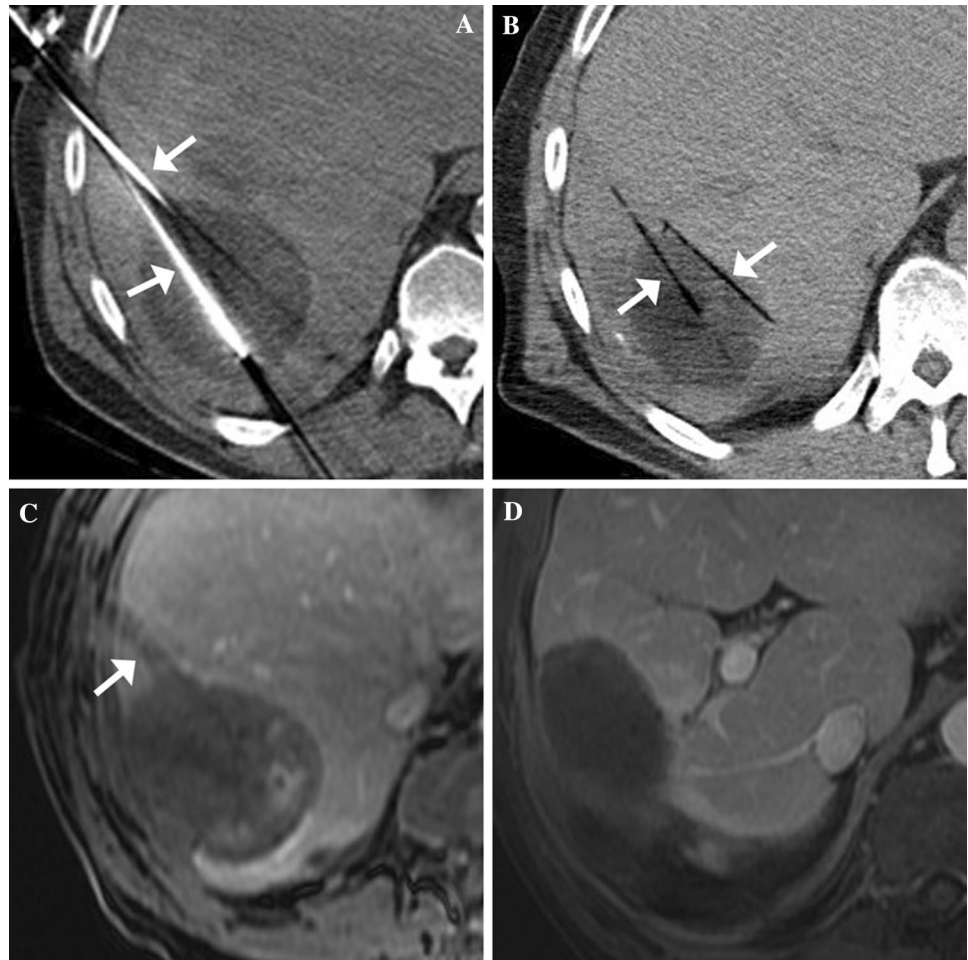
Fig. 5 Sixty-one-year-old man who underwent CT-guided cryoablation of a urothelial carcinoma metastasis. **a** Axial, intra-procedural, unenhanced CT image demonstrates two cryoablation probes in the target lesion with surrounding ice ball (arrows). **b, c, and d** Axial, 24-h, post-procedure, T1-weighted, fat-saturated, contrast-enhanced MR image in the arterial phase (**b**), portal venous phase (**c**), and delayed phase (**d**) shows ablation zone engulfing the mass with normal expected progressive hyper-enhancement of the tumor rim and ablation margin (arrows). **e** Axial, T1-weighted, fat-saturated, contrast-enhanced MR image obtained 3 months after cryoablation demonstrates resolution of hyperenhancement within the ablation zone without local recurrence (arrow)



techniques [9, 15, 23]. With cryoablation, high pressure argon gas is allowed to expand within the tip of a cryoprobe resulting in a temperature drop to approximately $-140\text{ }^{\circ}\text{C}$ at the probe tip (Joule–Thomson effect). The goal of cryoablation is to lower the temperature of the treated tissue volume below a threshold of $-20\text{ }^{\circ}\text{C}$ to $-40\text{ }^{\circ}\text{C}$ to ensure

cell death [24–27]. Ice initially forms outside the cell creating a hypertonic slush that causes cellular dehydration. Ice then develops inside the cell prompting cell membrane disruption; intra and extracellular ice then aggregates into a confluent ice ball [28]. A weakened cytoskeleton from mechanical shearing, cellular dehydration and osmotic

Fig. 6 Sixty-one-year-old male who underwent cryoablation of a hepatocellular carcinoma. **a** Axial, intra-procedural, unenhanced CT demonstrating the cryoprobes as linear metallic densities (arrows) with associated beam hardening artifact. **b** Immediate post-procedure CT after the cryoprobes were removed demonstrates linear hypodensities (arrows) due to air in the ablation tracts. **c** Axial, 24-h, post-procedure, T1-weighted, fat-saturated, contrast-enhanced MR image demonstrates a linear non-enhancing T1 hypointense ablation tract (arrow), an expected finding. **d** Axial, T1-weighted, fat-saturated, contrast-enhanced MR image obtained 3 months after cryoablation demonstrates resolution of the ablation tracts



shifts within endothelial cells lead to shape changes and detachment from the extracellular matrix causing intravascular thrombosis [29, 30]. Potentially sub-lethal temperatures at the periphery of the cryoablation zone leave a population of cells attempting to repair intracellular proteins and cell membrane lipoproteins; the end result may be activation of apoptotic mechanisms leading to cellular death or residual viable cells [28, 31, 32]. The principal mechanisms of cell death include direct (cellular dehydration and disruption from ice crystal formation and thrombosis of the microcirculation) and indirect (cellular apoptosis and inflammation) factors [4, 31, 33]. In addition, while coagulative necrosis occurs in the central ablation zone, at the periphery, inflammatory cells from the host response to injury induce neovascularity and eventual fibrosis [32]. Variations in cryoablation technique such as the rate of freezing and thawing, the number of freeze/thaw cycle repetitions, and the temperature and duration of freezing influence the effectiveness of cell kill [32, 34–36].

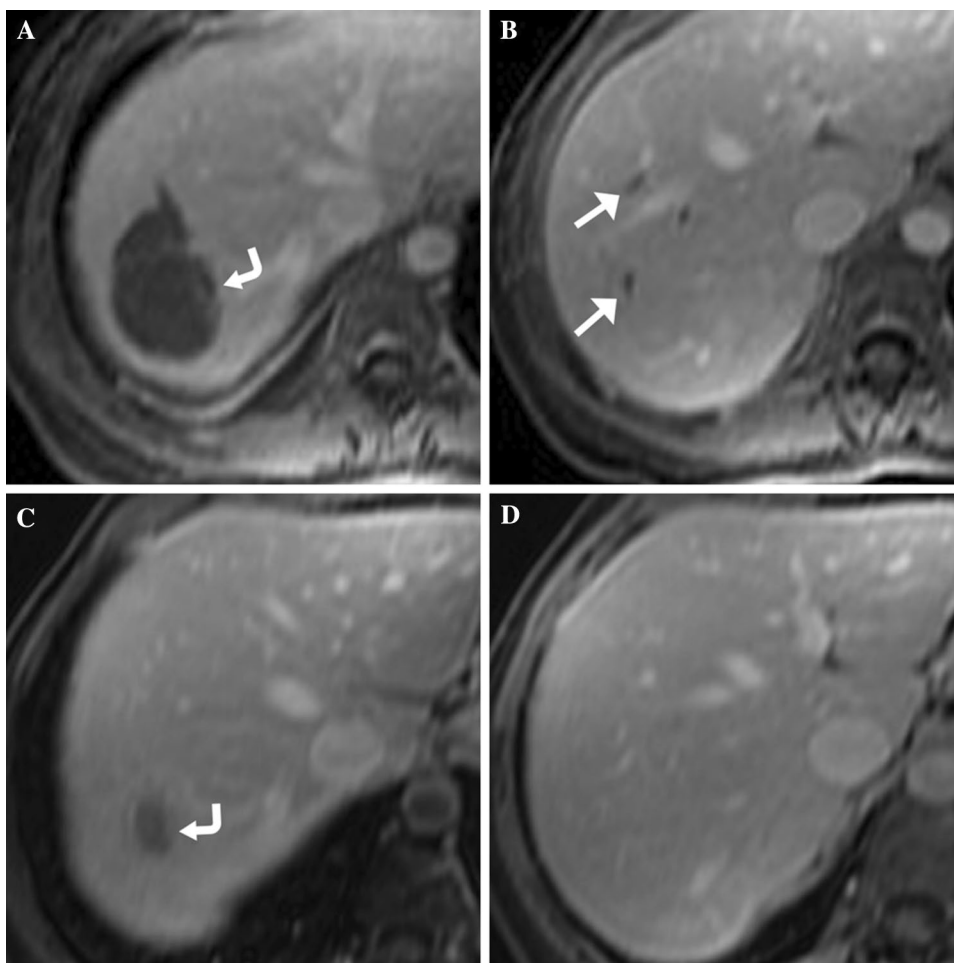
Expected findings

Intra-procedural

Ice ball formation

Intermittent intra-procedural imaging of the ice ball is performed with CT or MRI to monitor ice ball size such that the entire tumor is treated with a 5–10 mm minimum margin, as much liver parenchyma as possible is preserved, and nearby critical structures are avoided [24, 37, 38]. Ice balls are generally spherical or ovoid in shape depending on the type, number, and spatial arrangement of the cryoprobes. The size of the ice ball increases with longer freezing times and lower probe temperatures; the ice ball is controlled to optimize tumor coverage and margin adequacy. The size of an ice ball also increases synergistically with the use of additional probes, such that the ablation zone formed by two probes used simultaneously is larger than the sum of two separate probes [39]. Tissue type influences ice ball size; for example,

Fig. 7 Forty-six-year-old female who underwent cryoablation of an ovarian cancer metastasis. **a** and **b** Axial, 24-h, post-procedure, T1-weighted, fat-saturated, contrast-enhanced MR images demonstrates thrombosis of portal vein branches (arrows) adjacent to the ablation zone (curved arrow). **c** and **d** Axial, T1-weighted, fat-saturated, contrast-enhanced MR images obtained 6 months after cryoablation demonstrates shrinkage of the ablation zone (curved arrow) and resolution of portal venous thrombosis



fat has a lower freezing point. Increased tissue perfusion and the presence of heat sinks such as large blood vessels inhibit ice ball formation [37, 39]. The ice ball edge as seen on CT or MRI represents the 0 °C isotherm; lethal temperatures for liver tumors are thought to be located 5–10 mm within the initial ice ball and repeated freeze–thaw cycles move the lethal isotherm closer to the ice ball edge [39].

On CT images, the ice ball is hypoattenuating and sharply circumscribed relative to normal liver parenchyma [14] (Fig. 1). The ice ball may be less distinct from a hypodense tumor. Also, the ice ball is often isoattenuating and therefore less visible in fat. Modification of the window and level settings of the CT images may be required to improve the visual contrast between fat and the cryoablation zone [38]. On MRI images, the ice ball is seen as a signal void on virtually all pulse sequences. The signal void ice ball is visible in all tissues including fat and virtually any tumor; once engulfed by ice, all tissues including tumor are usually indistinguishable within the ice ball [16]. Although phantom and in vivo studies in canines

have shown specialized techniques such as ultra short echo time to be able to provide temperature dependent maps during cryoablation [40], we do not use this technique in our clinical practice.

Hydrodissection

To achieve an adequate ablation margin, the ice ball may extend beyond the liver and therefore affect other organs. During pre-procedure planning, critical structures such as the diaphragm, heart, gallbladder, stomach, and bowel near the target lesion should be identified and avoided if possible. If patient positioning does not result in optimal displacement of adjacent vulnerable structures, creation of artificial ascites (in the peritoneal space) or a salinoma (in soft tissues such as fat) may be attempted to displace the adjacent critical structures away from the planned ice ball [41].

Artificial ascites or salinoma is achieved by introducing a needle or catheter between the cryoablation target and the critical structure under image guidance and instilling

Fig. 8 Fifty-eight-year-old female who underwent cryoablation of a breast cancer metastasis. **a** Axial, intra-procedural, unenhanced CT image demonstrating cryoprobes and hypodense ice ball (arrows) at the site of the metastasis. **b** and **c** Axial, 24-h, post-procedure, T1-weighted, fat-saturated, contrast-enhanced MR images demonstrate area of wedge-shaped perfusion abnormality (arrows) adjacent to the ablation zone and ablation track on the arterial phase imaging (**b**), not seen on the portal venous phase images (arrows) (**c**). **d** Axial, T1-weighted, fat-saturated, contrast-enhanced MR image obtained 6 months after cryoablation in the arterial phase demonstrates resolution of the perfusion abnormality



Fig. 9 Seventy-six-year-old male with cirrhosis who underwent cryoablation of a hepatocellular carcinoma. **a** Axial, T1-weighted, fat-saturated, contrast-enhanced MR image obtained 3 months after cryoablation demonstrates mild biliary ductal dilatation (arrow) upstream to the ablation zone (curved arrow). **b** Axial, T1-weighted, fat-saturated, contrast-enhanced MR image obtained 6 months after cryoablation shows resolution of biliary dilatation and shrinkage of the ablation zone (curved arrow)

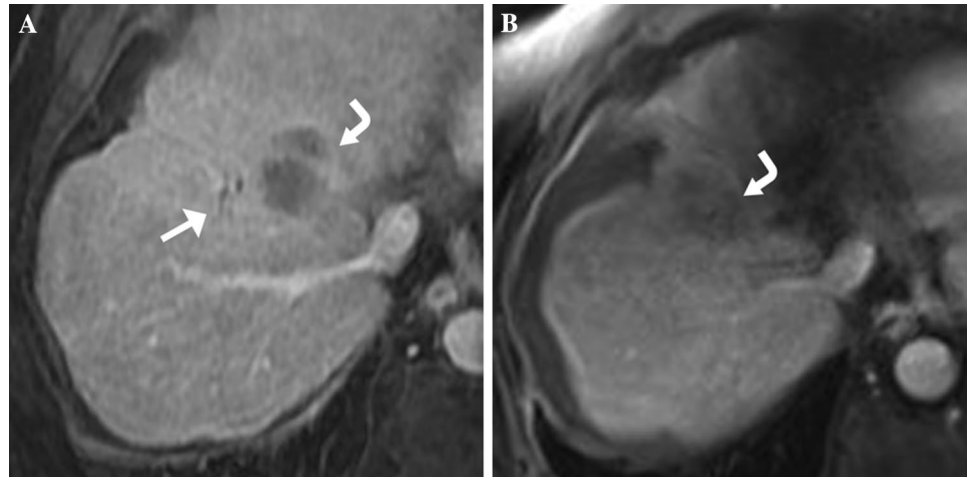
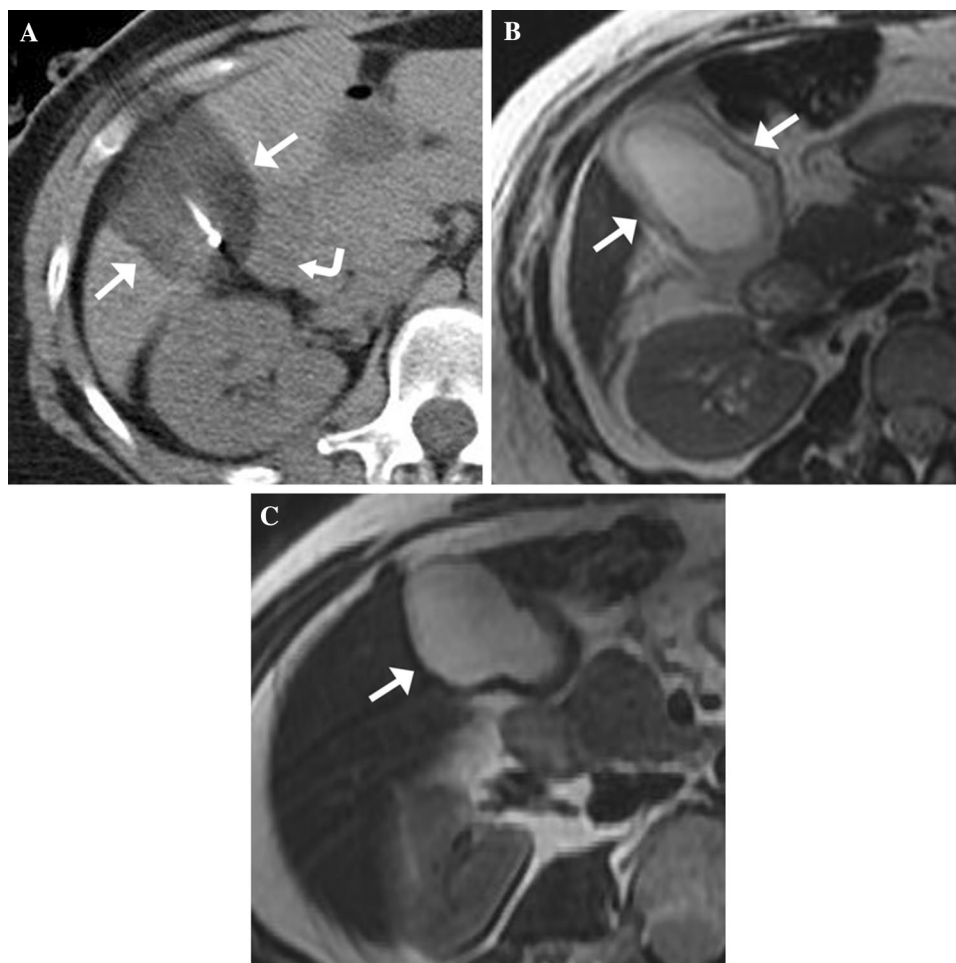


Fig. 10 Fifty-eight-year-old female who underwent cryoablation of a breast cancer metastasis adjacent to the gallbladder. **a** Axial, intra-procedural, unenhanced CT shows the ice ball (arrows) in close proximity to the gallbladder at its hepatic attachment (curved arrow). **b** Axial, 24-h, post-procedure T2-weighted MR image demonstrates asymptomatic gallbladder wall thickening (arrows). **c** Axial, T2-weighted MR image obtained 3 months after cryoablation demonstrates resolution of gallbladder wall thickening (arrow)



100–1000 mL or more of isotonic fluid such as normal saline to create adequate separation; adequacy of separation is assessed with imaging before commencing ablation and intermittently during the procedure. Because of redistribution of fluid within the peritoneal space, continuous instillation may be required (Fig. 2). Note that if dilute contrast is used, the ice ball may not be well seen within this fluid. 24-h imaging may show variable amounts of residual fluid near the target organ or remote from the target organ due to patient movement and depending on the rate of absorption and volume of fluid used [42–44]. The fluid is eventually resorbed in all patients.

Post-procedural

Hemorrhage (immediate)

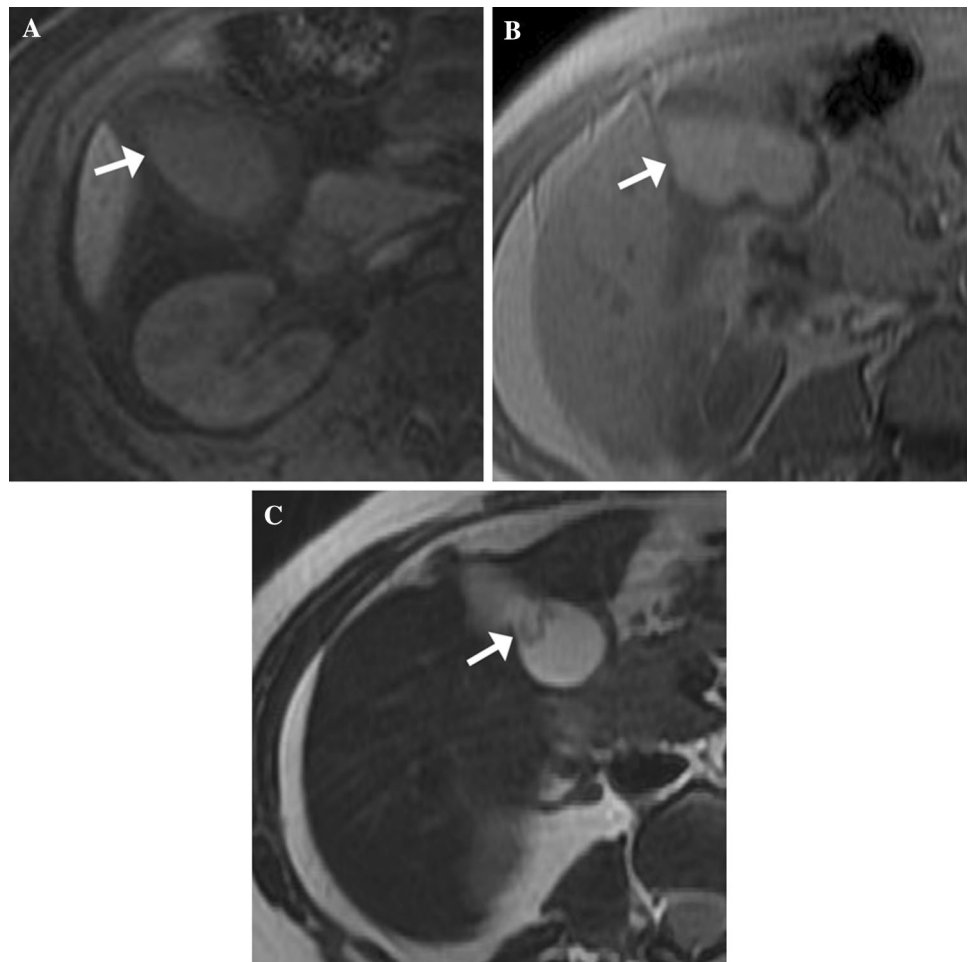
Hemorrhage may result from probe passage through the highly vascular liver especially with multiple punctures. Bleeding is usually self-limited unless a visible blood vessel

is actually punctured. Hemorrhage is isodense to hyperdense on CT. Its appearance ranges from isointense to hyperintense on unenhanced T1-weighted MR images depending on the hemoglobin content and is usually hypointense on T2-weighted MR images (Fig. 3). These findings can persist to a variable degree and may evolve over several weeks after the procedure [45].

Ablation zone (immediate to months)

The ablation zone is the term used to describe the radiologic region of induced treatment effect or the area of gross tissue destruction visualized on imaging [46]. After ablation, imaging findings vary by location: (1) the ablation zone, (2) the periphery of the ablation zone, or (3) the normal tissues adjacent to the ablation zone. Also imaging appearances after cryoablation are dynamic over time [30] hence it is helpful for the radiologist to know the time interval since cryoablation.

Fig. 11 Sixty-year-old female who underwent cryoablation of an ovarian cancer metastasis near the gallbladder. **a** Axial, 24-h, post-procedure, T1-weighted, fat-saturated, MR image demonstrates layering of hyperintense blood (arrow) in the gallbladder. **b** and **c** Axial, T1-weighted MR image obtained 3 months after cryoablation **b** demonstrates layering hyperintense hemorrhage in the gallbladder (arrow) and axial T2-weighted MR image **c** shows retractile clot within the gallbladder (arrow)



Heterogeneous signal changes on MRI may be observed within the ablation zone which should extend 5–10 mm beyond the tumor [15, 39] (Fig. 4). Coagulative necrosis within the ablation zone may appear T1-hyperintense and T2-hypointense due to T1 shortening effects of extracellular proteins and desiccation. More commonly, the ablation zone at 24 h appears T1-hypointense and heterogeneously T2-hyperintense. If markedly T2-hyperintense, fluid may be accumulating; if fluid is present and/or expanding the ablation zone, the possibility of a biloma should be considered. Foci of T1 hyperintense/T2 hypointense blood products or, more likely, coagulated proteins may contribute to the heterogeneity of the ablation zone and may persist for several months [36, 45].

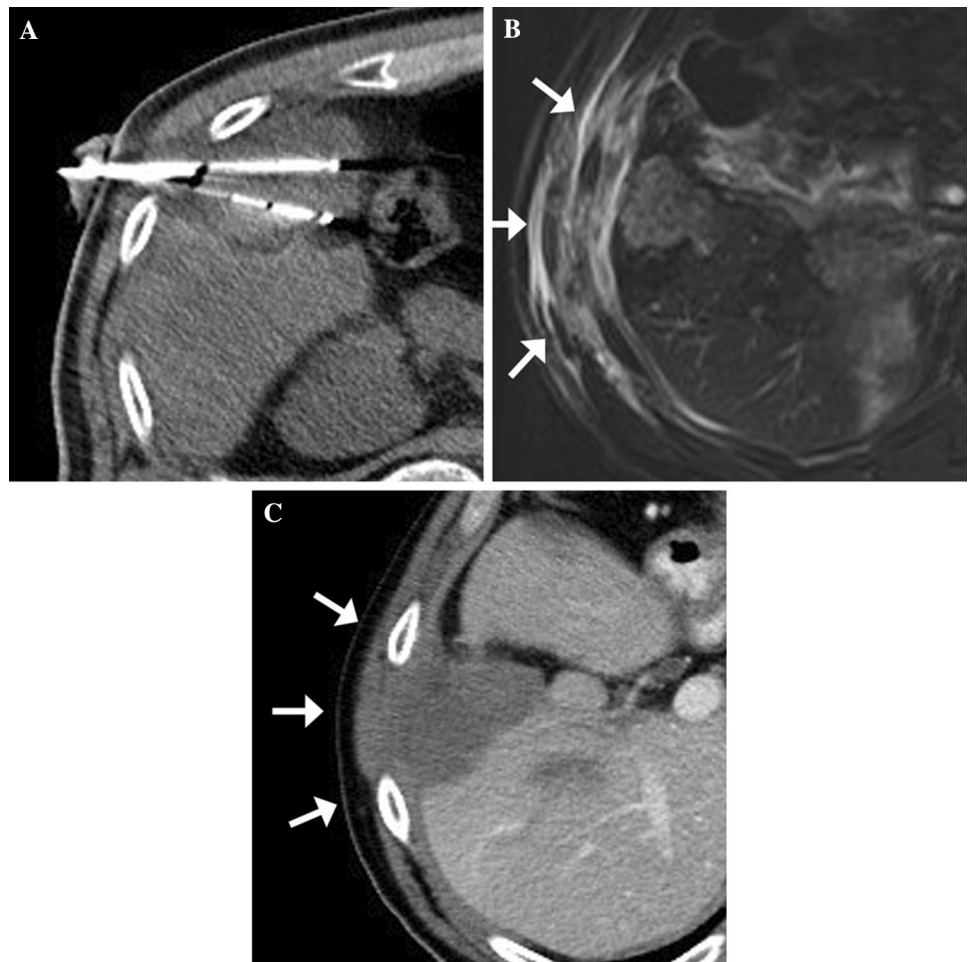
The periphery of the ablation zone is subject to an intense inflammatory response representing the physiologic response to thermal injury [46, 47]. In the immediate phase, edema, hyperemia, and reperfusion of damaged blood vessels result in T1 hypointense and T2

hyperintense signal in the periphery on MRI. Granulation tissue formation that begins at 24 h followed by fibrosis and angiogenesis, results in persistent smooth peripheral enhancement known as benign periablational enhancement (or the transitional zone) on both CT and MRI. Benign periablational enhancement manifests as a thin rim on early phases which becomes thicker on later phases [15] and typically resolves in 4–6 months [45] (Fig. 5). A fibrous capsule at the periphery of the ablation zone may form after 3 months but as late as 8–12 months. This fibrous capsule may enhance but demonstrates pre-contrast T1 and T2 hypointense signal. The capsule may allow the edge of the ablation margin to be defined on later follow-up imaging [15].

Ablation tract (immediate to several months)

Intra-procedural monitoring shows the cryoprobe as a metallic linear density on CT with associated beam hardening

Fig. 12 Sixty-three-year-old male who underwent cryoablation of a colon cancer metastasis. **a** Axial, intra-procedural, unenhanced CT image demonstrates cryoprobes and ablation zone in the right hepatic lobe. **b** Axial, 24-h, post-procedure, T2-weighted MR image shows edema and inflammatory changes in the soft tissues (arrows) related to mechanical trauma by the cryoprobe and freeze injury. **c** Axial, contrast-enhanced CT image obtained 3 months after cryoablation demonstrates near-resolution of soft tissue changes (arrows)



artifact or as a signal void on MRI images. After removal, on post-procedural imaging, a linear tissue tract is often seen in the location of the cryoprobes. The tract is non-enhancing and results from traversing the hepatic parenchyma (Fig. 6). Because the ice ball forms principally at the distal end of newer insulated probes, there is generally little additional effect along the cryoprobe shaft. However perfusion abnormalities may result in wedge-shaped hyperenhancement along its course [48]. Visibility of the probe tract often resolves on successive follow-up exams [16].

Vascular changes (immediate to several months)

Vascular changes on post-procedure imaging may result from cryoablation-induced vascular injury or mechanical trauma by the cryoprobe, and small vessels are more susceptible to freeze injury than larger ones. As early as the first post-procedure day, non-enhancing T1 hyperintense portal vein branches may be seen along the ablation tract or

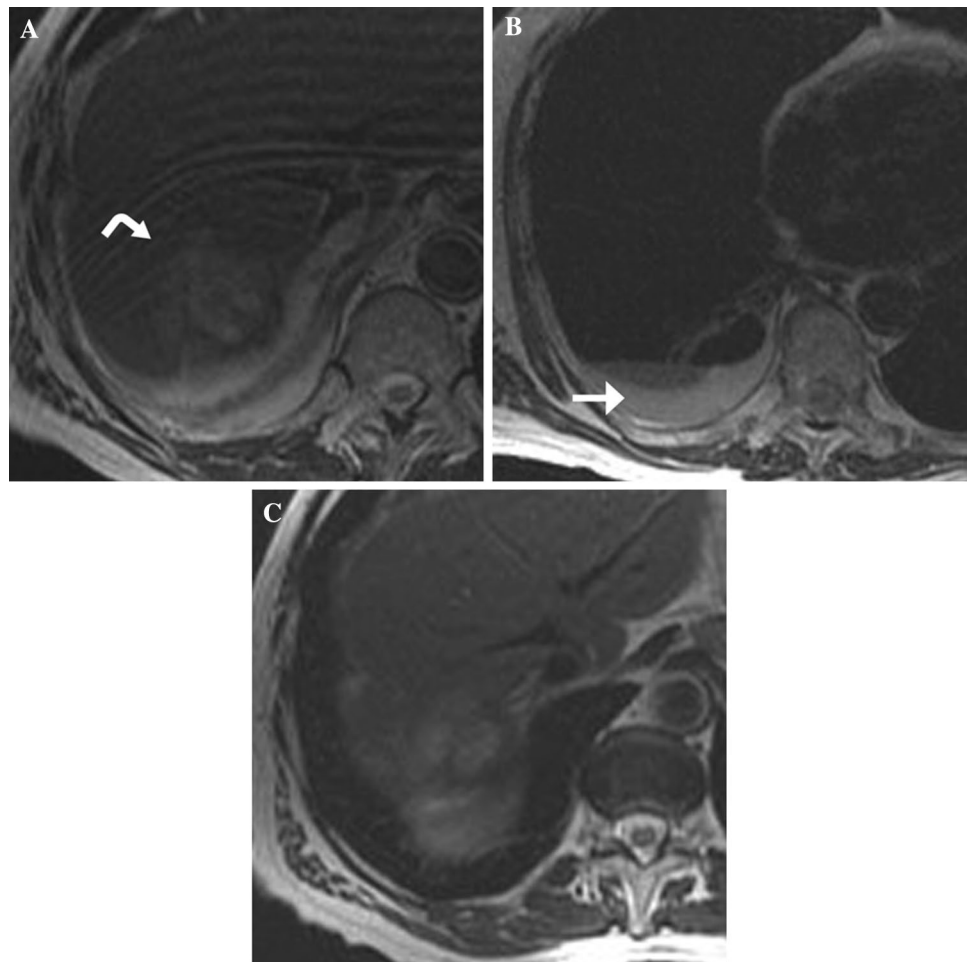
adjacent to the ablation zone as venous stasis leads to thrombosis. Reports have shown venous thrombosis occurring approximately 20% of the time on immediate 24-h imaging, affecting vessels with an average diameter of 4 mm, with either complete or partial recanalization at 3 months follow-up (Fig. 7) [49].

Wedge-shaped or geographic hyperenhancement of liver parenchyma may be seen on arterial phase images, likely representing compensatory hepatic artery hyperperfusion in the distribution of reduced portal venous perfusion (Fig. 8). These vascular changes are temporary and usually resolve over the course of 4–6 months without clinical sequelae [36, 48, 50].

Biliary changes (immediate to several months)

The biliary system, supplied by a capillary plexus from the hepatic arterial system and without dual vascular supply, is susceptible to the effects of tissue freezing [51]. As seen

Fig. 13 Fifty-five-year-old man who underwent cryoablation of a colorectal cancer metastasis at hepatic dome. **a** and **b** Axial, 24-h, post-procedure, T2 weighted MR images shows ablation zone at the hepatic dome (curved arrow) and small right pleural effusion (straight arrow). **c** Axial, T2-weighted MR image obtained 3 months after cryoablation shows resolution of the right pleural effusion



in other ablative therapies [52], focal biliary ductal dilation upstream to the ablation zone can result from biliary stasis and outflow obstruction. The time of appearance after ablation is variable but is usually transient and may resolve as the ablation zone involutes (Fig. 9). The effects on the biliary tree are largely dependent on the size of the ducts that are affected; the more central the ducts, the more likely there will be clinical sequelae such as obstruction or bile leak.

Cryoablation of tumors near the gallbladder can be performed safely and effectively even if the ice ball extends into the hepatic attachment of the gallbladder [53]. Changes such as focal gallbladder wall thickening, pericholecystic fat stranding and fluid related to transient mild cholecystitis have been described in a limited series, with minimal morbidity [53]. These findings are usually self-limiting and resolve spontaneously on follow-up imaging (Fig. 10). On the other hand, freezing the peritoneal surface of the gallbladder can lead to bile leak and

peritonitis. Arterio-biliary injury can cause bleeding into the bile ducts and gallbladder, leading to visible blood products within biliary structures and even biliary obstruction (Fig. 11) [54].

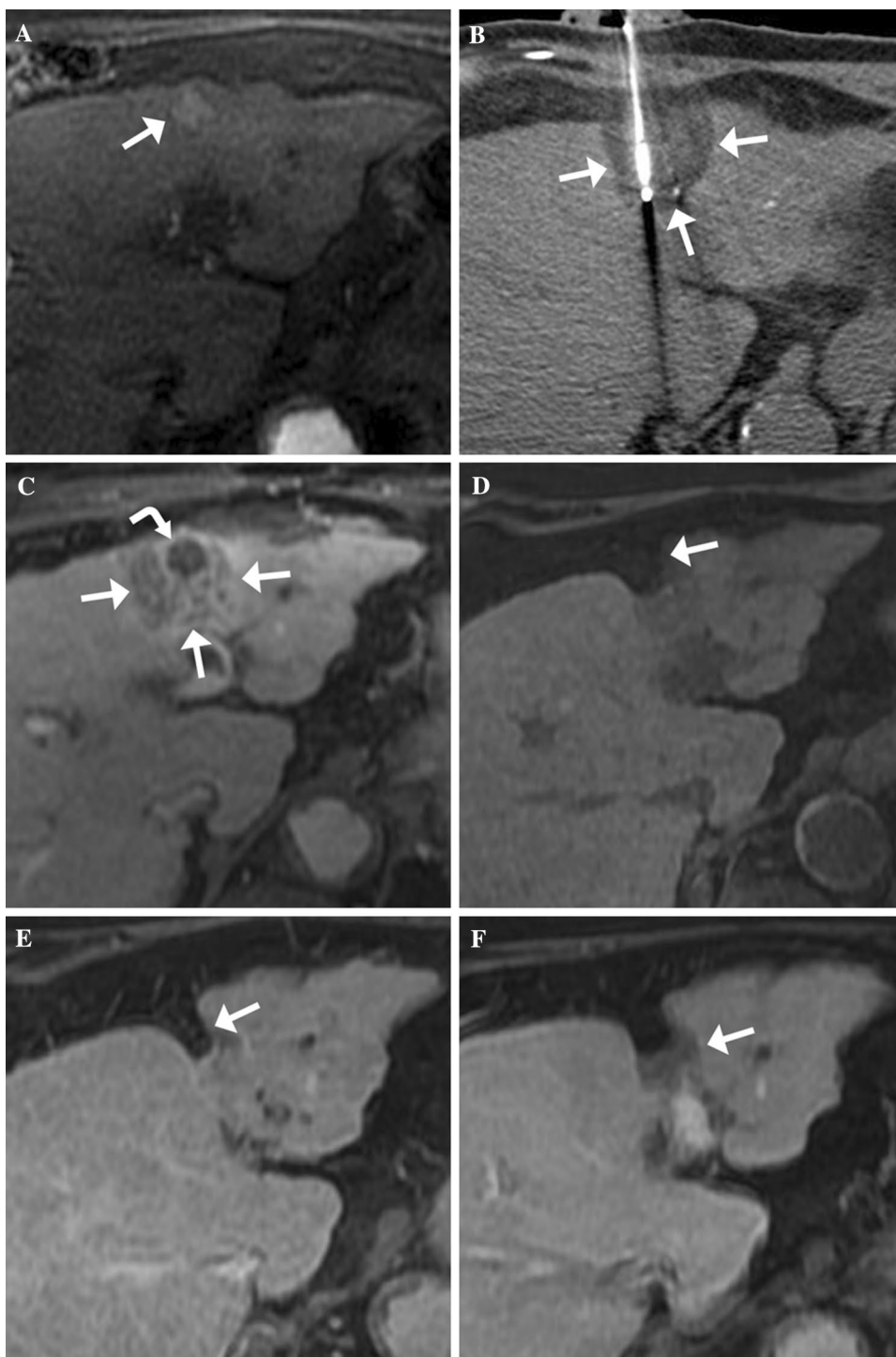
Soft tissue changes (immediate)

Soft tissue changes outside the liver and along the track of cryoprobes may include peri-hepatic fat stranding or hematoma due to cryoprobe injury. Hepatic ablation zone imaging findings may extend into surrounding soft tissues if the ice ball was not confined to the liver; these findings gradually diminish over months (Fig. 12) [55].

Pleural effusion (immediate)

An ipsilateral pleural effusion may develop after cryoablation even if the pleural space is not violated, particularly if the treated lesion is located in the liver dome or if the ice

Fig. 14 Seventy-six-year-old female with cirrhosis who underwent cryoablation of a hepatocellular carcinoma. **a** Axial, pre-procedure, T1-weighted, fat-saturated, contrast-enhanced MR image in the arterial phase demonstrates a cirrhotic liver with a hyper-enhancing mass in the left lobe concerning for hepatocellular carcinoma. **b** Axial, intra-procedural, unenhanced CT image demonstrates cryoprobe in the target lesion with surrounding ablation zone (arrows). **c** Axial, 24-h, post-procedure, T1-weighted, fat-saturated, contrast-enhanced MR image demonstrates delayed enhancement within the ablation zone (arrows) surrounding the target lesion (curved arrow) which also shows rim enhancement. **d, e, and f** Axial, T1-weighted, fat-saturated, contrast-enhanced MR image demonstrates progressive retraction of the liver capsule (arrow) over 6 months (**d**), 9 months (**e**), and 12 months (**f**) without local recurrence

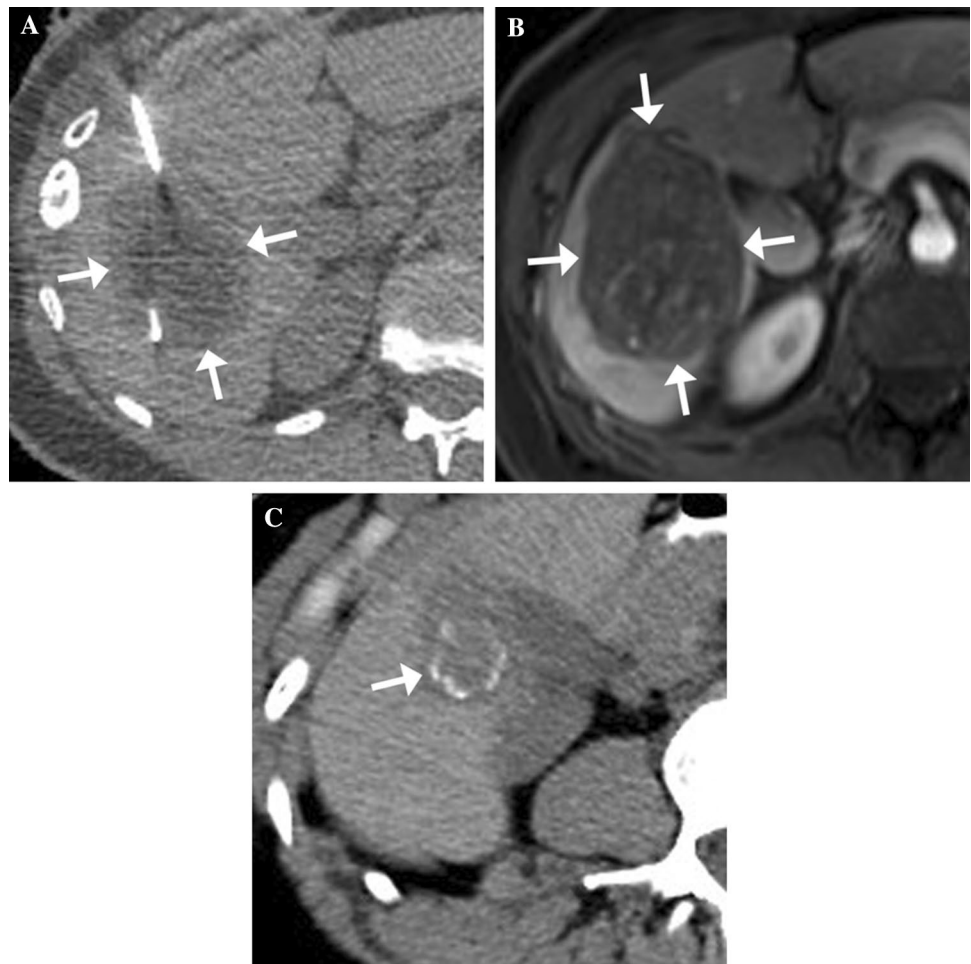


ball involves the diaphragm (Fig. 13). Although injury to diaphragmatic vessels is postulated as a possible cause, a reactive phenomenon has also been implicated as contralateral pleural effusions sometimes develop. The effusions are typically small to moderate, asymptomatic, and resolve spontaneously [33, 56].

Involution, capsular retraction, calcification (months)

On follow-up CT and MRI examinations at 2 to 3 months or more, fibrous scarring and tissue resorption result in involution of the ablation zone. Involution of the ablation zone is more pronounced with cryoablation than heat-based

Fig. 15 Forty-year-old female who underwent cryoablation of a breast cancer metastasis. **a** Axial, intra-procedural, unenhanced axial CT image demonstrates cryoprobe within the target lesion and surrounding ice ball (arrows). **b** Axial, 24-h, post-procedure, T1-weighted, fat-saturated, contrast-enhanced MR image demonstrates hypoenhancing ablation zone (arrows). **c** Axial CT image obtained 12 months after cryoablation shows dystrophic calcification (arrow) within the involuting ablation zone



ablations [57]. Following ablations at the periphery of the liver, liver capsular retraction may result, causing a contour defect (Fig. 14). In rare instances, dystrophic calcification may form within the scarred ablation zone (Fig. 15) which should be well-margined with no associated enhancement.

Unexpected findings

Narrow margin

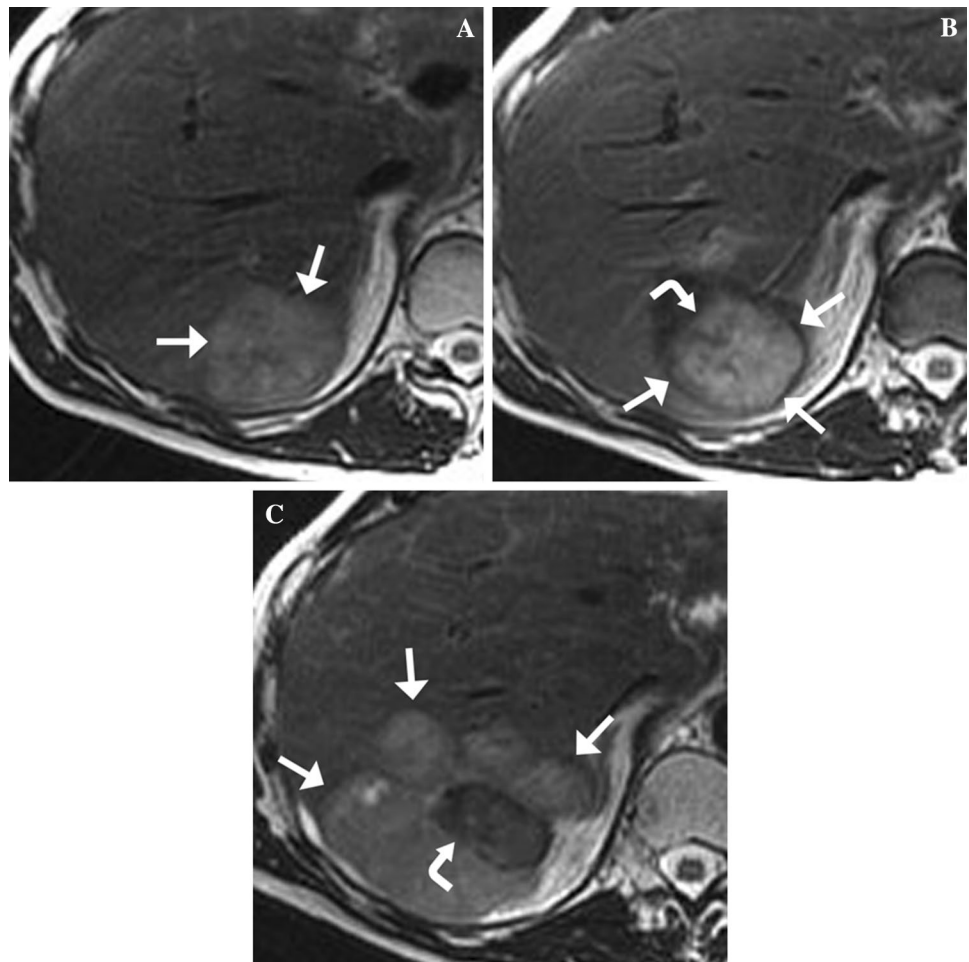
Theoretically, the lethal isotherm is 5–10 mm within of the ice ball edge and thus the ice ball should ideally extend 10 mm beyond the edge of the tumor [39, 58]. An adequate margin is believed to ensure that microscopic tumor beyond the visible tumor margin is ablated. Multiple freeze–thaw cycles tend to move the lethal isotherm close to the ice ball edge. Although 10 mm is ideal, the minimum ablation margin needed is not entirely known; one study suggested that

cryoablation margins less than 3 mm predict local tumor progression [15]. Nevertheless, one of the most important observations to be made on immediate post-procedure imaging is whether the hypoenhancing ablation zone extends sufficiently beyond the tumor in all dimensions. The adequacy of the ablation zone is assessed by measuring the minimum ablation margin on whichever contrast-enhanced MRI sequence best shows the tumor ‘ghost’ and ablation zone. In most, but not all cases, the margin can be assessed either on a contrast-enhanced image obtained at the end of the procedure or at 24-h. Detection of a narrow margin requires close attention at follow-up imaging (Fig. 16) [59].

Residual unablated tumor

Residual unablated tumor refers to residual tumor at the ablative margin seen on the initial follow-up imaging [46]. The risk of residual unablated tumor is high when the ablative margin is narrow or absent [15]. In patients with

Fig. 16 Fifty-five-year-old male who underwent cryoablation of a colorectal metastasis with narrow ablation zone increasing risk of recurrence. **a** Axial, pre-procedure T2-weighted MR image showing mildly T2 hyperintense metastasis (arrows) in the right hepatic lobe. **b** Axial, 24-h, post-procedure, T2-weighted MR image shows hypointense ablation zone (arrows) engulfing the T2 hyperintense mass (curved arrow) with narrow minimum margins, much less than 1 cm. **c** Axial, T2-weighted MR image obtained 3 months after cryoablation shows multiple, new peripheral T2 hyperintense tumor nodules (arrows) around the ablation zone (curved arrow)



hepatocellular carcinoma, larger tumors are more frequently associated with microscopic satellite tumor nodules adjacent to the dominant tumor, which may be subtle or invisible [60]. An advantage of cryoablation is that both the tumor ‘ghost’ and cryoablation zone are often visible on 24-h post-procedure MRI. Visibility of both the tumor and the ablation zone allows measurement of the minimum ablation margin. Identification of an absent margin or residual tumor may prompt earlier follow-up or retreatment [15].

Comparison of pre-ablation images with post-ablation images is important for recognizing residual unablated tumor. In contrast to the smooth concentric appearance of benign periablation enhancement, unablated residual tumor demonstrates irregular peripheral enhancement that can be scattered, nodular, or eccentric on CT and MRI [47]; it can focally widen the surrounding zone of granulation tissue or disrupt the typical smooth interface of the ablation zone with surrounding normal hepatic parenchyma [61, 62]. Sub-lethal temperatures near the periphery of the ablation

zone may contribute to this potential pattern of residual disease. As the T2 hyperintense, enhancing granulation tissue regresses on subsequent follow-up, the enhancing nodular tumor becomes more conspicuous [36]. In addition, subtraction images which digitally remove native hyperintense signal on unenhanced T1-weighted images can improve visibility of enhancing residual unablated tumor [63].

Local tumor progression

An enhancing nodule appearing within or more commonly at the margin of the ablation zone of a treated lesion, after at least one contrast-enhanced follow-up exam has documented adequate ablation and an absence of enhancing tissue in the target tumor and surrounding ablation margin suggests local tumor progression [46]. In some cases, it is not possible to distinguish local tumor progression from local tumor recurrence; the latter defined as new tumor growth at the ablative margin after local eradication of all

Fig. 17 Fifty-five-year-old female history of cirrhosis who underwent cryoablation of a hepatocellular carcinoma. **a** Axial, pre-procedure, T1-weighted, fat-saturated, contrast-enhanced MR image in the arterial phase demonstrates an enhancing mass (arrow) in left hepatic lobe consistent with hepatocellular carcinoma. **b** Axial, intra-procedural, unenhanced CT with cryoprobes and hypodense ablation zone (arrows) surrounding the mass and extending into the body wall. **c** Axial, 24-h, post-procedure, T1-weighted, fat-saturated, contrast-enhanced MR image showing the ablation zone with peripheral enhancement (arrows). **d** Axial, T1-weighted, fat-saturated, contrast-enhanced MR image obtained 3 months after cryoablation shows an enhancing nodule (arrow) in the periphery of the ablation zone concerning for local tumor progression

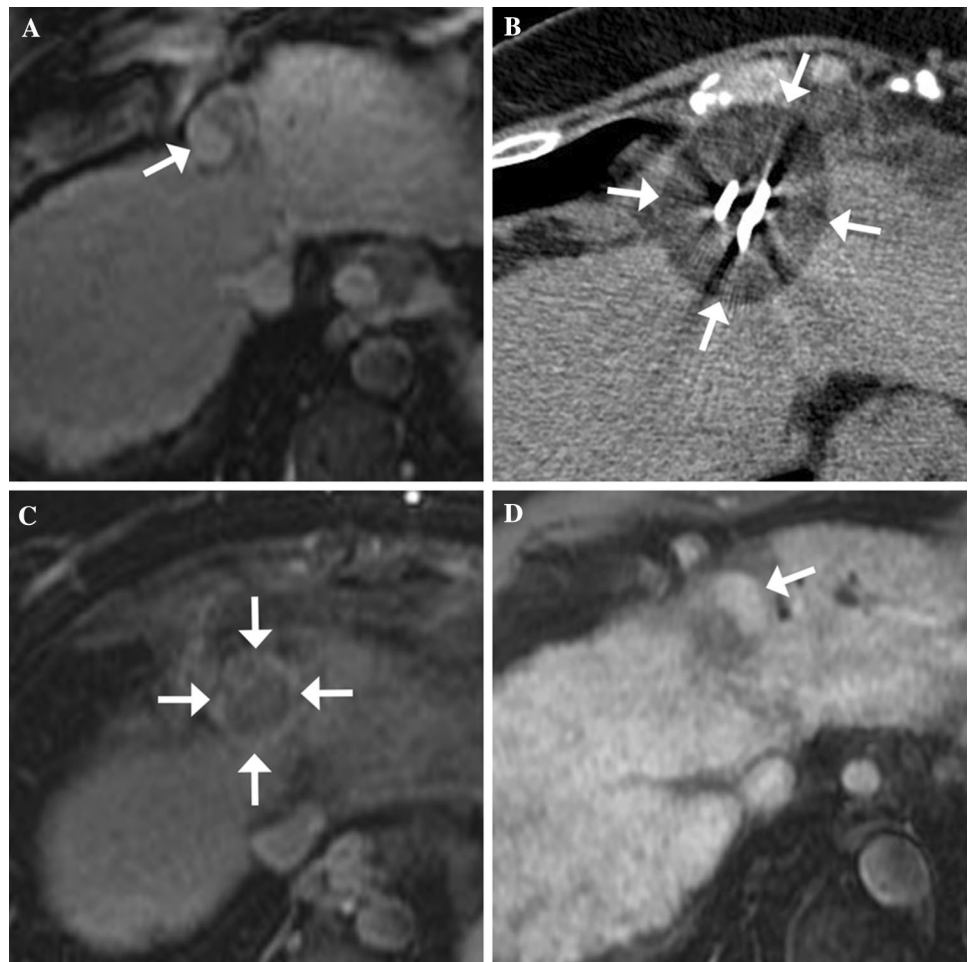
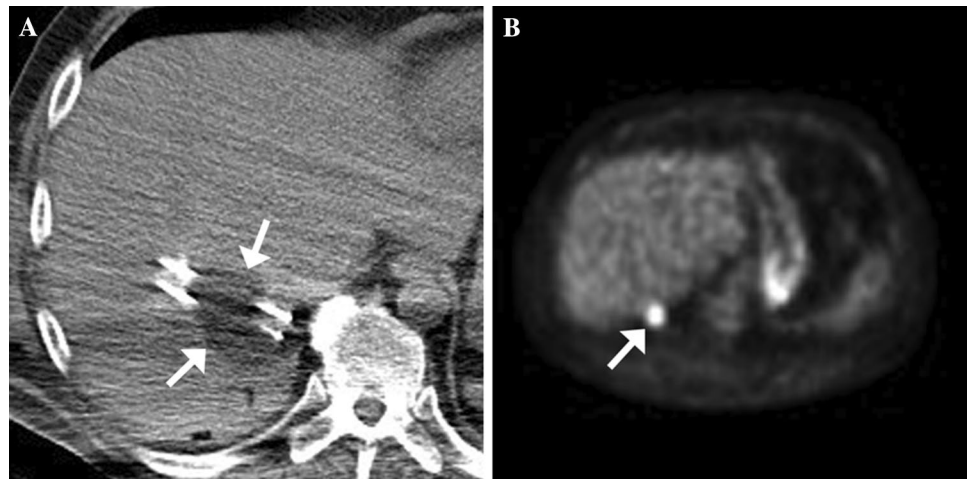


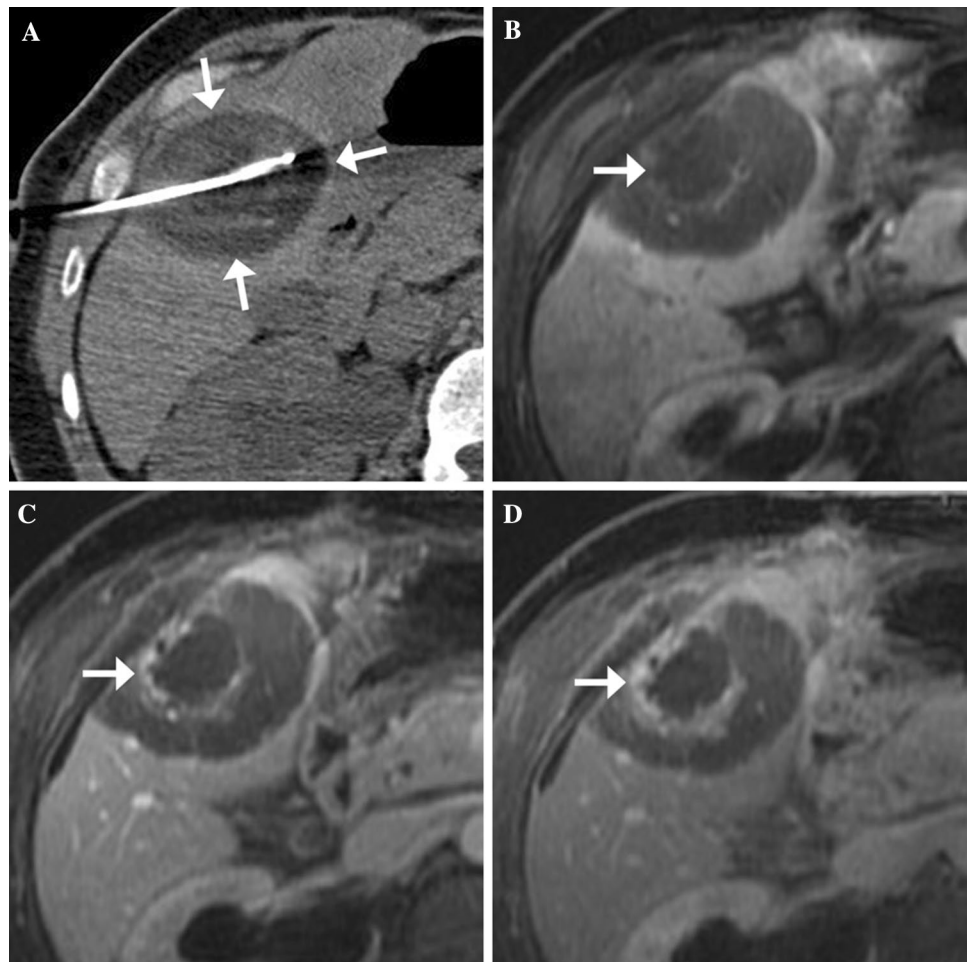
Fig. 18 Fifty-five-year-old male who underwent cryoablation of a rectal cancer metastasis. **a** Axial, intra-procedural, unenhanced CT image demonstrates cryoprobes at the target lesion and surrounding ablation zone (arrows). **b** PET/CT obtained 6 months after cryoablation shows FDG-avid lesion at the periphery of ablation zone (arrow) concerning for local tumor progression



tumor cells by ablation [46]. Tumor at the ablative margin is thought to more often signify remaining untreated microscopic tumor rather than a new local recurrence [46]. Local tumor progression typically appears similar to the original

tumor [64] (Fig. 17). Subtraction images can help improve detection of enhancing tumor [63]. In some instances, FDG PET-CT may be useful in the detection of local tumor progression (Fig. 18).

Fig. 19 Forty-six-year-old female who underwent cryoablation of an ovarian cancer metastasis. **a** Axial, intra-procedural, unenhanced CT image shows cryoprobes and ablation zone (arrows) surrounding the target lesion. **b, c, and d** Axial, 24-h, post-procedure, T1-weighted, fat-saturated, contrast-enhanced MR images in the arterial (**b**), portal venous (**c**), and delayed (**d**) phases demonstrate the ablation zone engulfing the mass with progressive peripheral enhancement of the ablated tumor (arrows); this is not an unexpected finding and is thought to be due to reperfusion of damaged vessels and leaky vasculature. This does not indicate residual or recurrent disease and often resolves over 4–6 months. The ablation margin is best assessed on early dynamic phase images



Persistent tumor enhancement

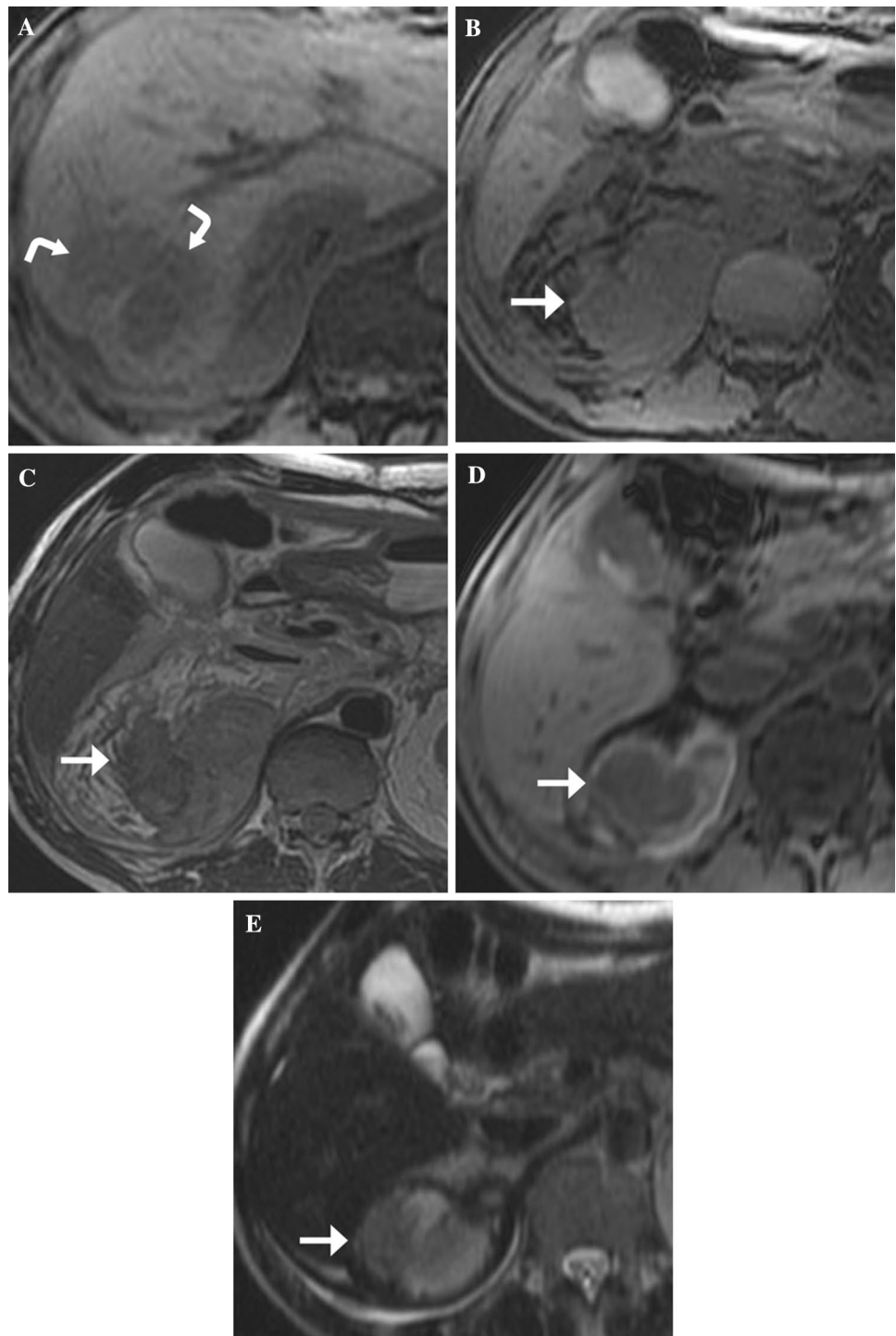
Progressive and persistent enhancement may be observed in fully cryoablated tumors and the surrounding ablation margin during early follow-up, typically at 24 h [15] (Fig. 19). The enhancement is usually less than normal liver in the arterial phase, gradually increasing into the delayed (5-minute) phase; it is postulated to be due to reperfusion of damaged, leaky vessels, and may be peripheral with a thick rim, peripheral with a thin rim, homogenous, inhomogenous, or with centripetal filling [15]. This is not predictive of incomplete ablation and tends to decrease or resolve over 4–6 months as long as an adequate hypoenhancing margin is demonstrated in the arterial or venous phase [15, 65].

Tumor seeding

Although we encountered no cases of tumor seeding after percutaneous liver cryoablation, it has been described after

percutaneous liver radiofrequency ablation [66]. Early reports of a small series of patients with HCC who had undergone radiofrequency ablation reported a seeding rate of as high as 12% [67], while later studies have reported a much lower seeding rate of between 0.9 and 2.7% [66, 68]. Thus attention must be paid to tissues along the ablation probe tract to assess for this unexpected finding, with risk factors including subcapsular lesions defined as being located less than 1 cm of the liver edge, multiple treatment sessions, and multiple electrode placements [66]. This is of particular importance in patients with hepatocellular carcinoma awaiting transplantation as needle track seeding resulting in peritoneal dissemination could make the patient ineligible for transplantation [69]. On imaging, tumor seeding can manifest as enhancing, irregular soft tissue along the ablation track [70]. This appearance can be mimicked by post-ablation inflammatory changes or granulation tissue; follow-up imaging or biopsy can be used to distinguish the possibilities [71].

Fig. 20 Fifty-seven-year-old man who underwent cryoablation of a peripheral hepatocellular carcinoma. **a**, **b**, and **c** Axial, 24-h, post-procedure, T1-weighted (**a**, **b**) and T2-weighted (**c**) MR images demonstrates ablation zone (curved arrows) at the right liver margin and large T1 isointense and T2 heterogeneous retroperitoneal hemorrhage (straight arrows). **d** and **e** Axial, T1-weighted (**d**) and T2-weighted (**e**) MR images obtained 3 months after cryoablation shows evolving retroperitoneal hemorrhage (arrows)



Complications

Vascular

A small amount of hemorrhage after cryoablation may occur and is usually limited. Factors that can increase the

risk of hemorrhage include the use of larger probes (16 G or thicker), multiple punctures when placing the probes, relatively longer treatment times, ablations near large blood vessels and presence of coagulation abnormalities. Management of active bleeding or large hematomas depends on clinical circumstances and may prompt further imaging

Fig. 21 Sixty-three-year-old female who underwent cryoablation of a hepatocellular carcinoma. **a** Axial, 24-h, post-procedure, T1-weighted, fat-saturated, contrast-enhanced MR image demonstrates ablation zone (arrow) and thrombus in the adjacent left portal vein (curved arrow). **b** Axial, T1-weighted, fat-saturated, contrast-enhanced MR image obtained 9 months after cryoablation demonstrates chronic thrombus with attenuation of the left peripheral portal vein but without central propagation (arrow)

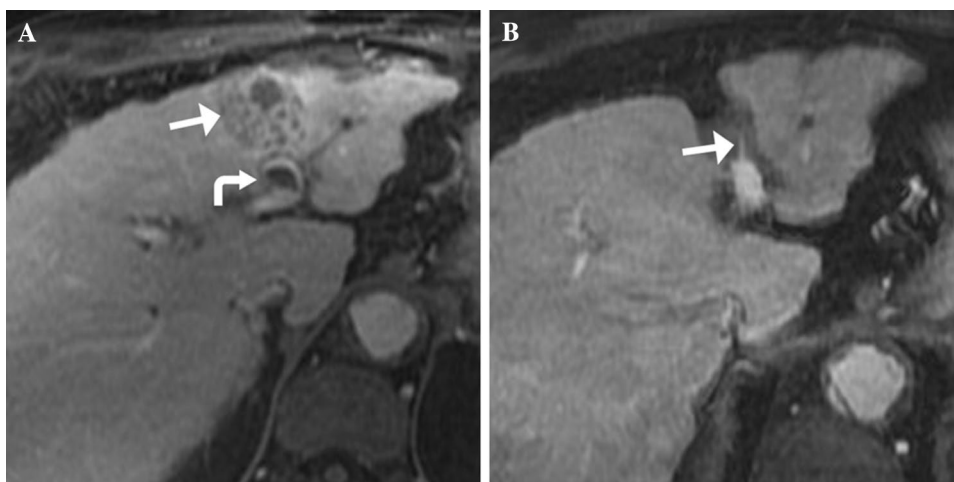
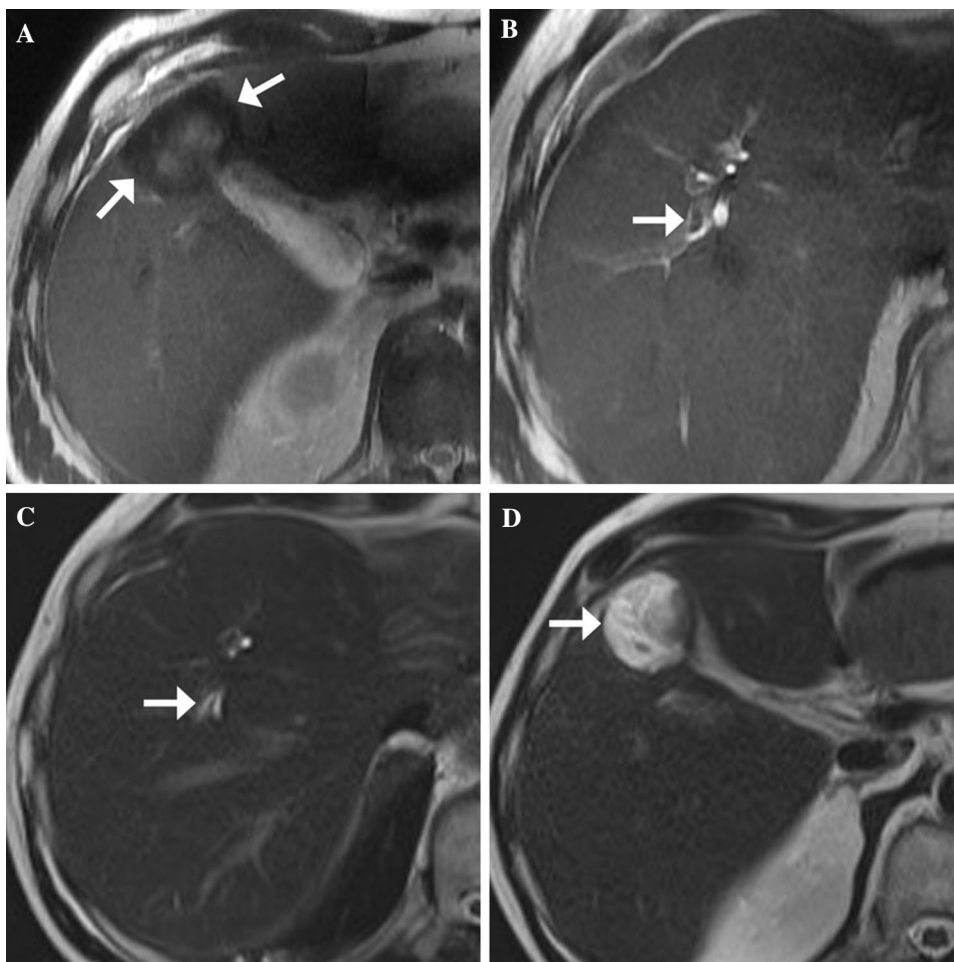


Fig. 22 Fifty-nine-year-old female who underwent cryoablation of a gastrointestinal stromal tumor metastasis. **a** Axial, T2-weighted MR image obtained 3 months after cryoablation shows ablation zone in segment 5 (arrows). **b** and **c** Axial, T2-weighted MR images shows upstream biliary ductal dilatation (arrows) at 3 months post-procedure imaging (**b**) which persists on 6 months post-procedure MRI (**c**). **d** Axial, T2-weighted MR image shows a well-circumscribed hyperintense biloma (arrow) adjacent and inferior to the ablation zone (**a**)



and/or interventional procedures (Fig. 20) [72]. Branch portal vein thrombosis is a relatively common finding on post-procedure imaging and is almost always asymptomatic with spontaneous resolution. Occlusion of portal veins may persist in rare cases (Fig. 21). Initial findings of

non-enhancing thrombus within the affected vessel may later lead to attenuation of the affected portal vein branch causing perfusional anomalies, regional atrophy, and collateralization/cavernous transformation if the affected vessel is large [50].



Fig. 23 Axial, 24-h, post-procedure, T1-weighted, fat-saturated, contrast-enhanced MR of an ovarian cancer metastasis shows the ablation zone (straight arrows) and non-target small area of ablation into the adjacent kidney (curved arrow)

Biliary

Dilation of the biliary system may be due to mass effect by the ablation zone or stricture formation due to thermal injury of the bile ducts. T2-hyperintense dilated ducts in a zonal distribution without abnormal enhancement and tapering near the ablation zone is the imaging hallmark. The time course is variable: while shrinkage of the ablation zone eventually may relieve an obstruction, ductal dilation may persist (Fig. 22). Although data from a cryoablation series are not available, the RFA literature shows bile duct changes occur in 12% of procedures [52]. Of RFA cases resulting in bile duct changes, mild bile duct dilatation upstream to the ablation zone occurred approximately 82% of the time with worsening on further follow-up in only 13% [52].

Severe direct injury to a large bile duct combined with necrosis of the adjacent ablated tumor may manifest with leakage of bile into the cavity and formation of a collection of bile (biloma). In a retrospective review of 3284 patients

Fig. 24 Sixty-six-year-old male who underwent cryoablation of a hepatocellular carcinoma. **a** and **b** Axial, 24-h, post-procedure, T2 weighted MR images demonstrate ablation zone at the hepatic dome (straight arrows), non-target lung ablation (curved arrows), and pleural effusion (black arrow). **c** and **d** Coronal and sagittal, T1-weighted, fat-saturated, contrast-enhanced MR images show ablation zone (straight arrows) with non-target ablation of the lung (curved arrow). The patient recovered without clinical sequelae

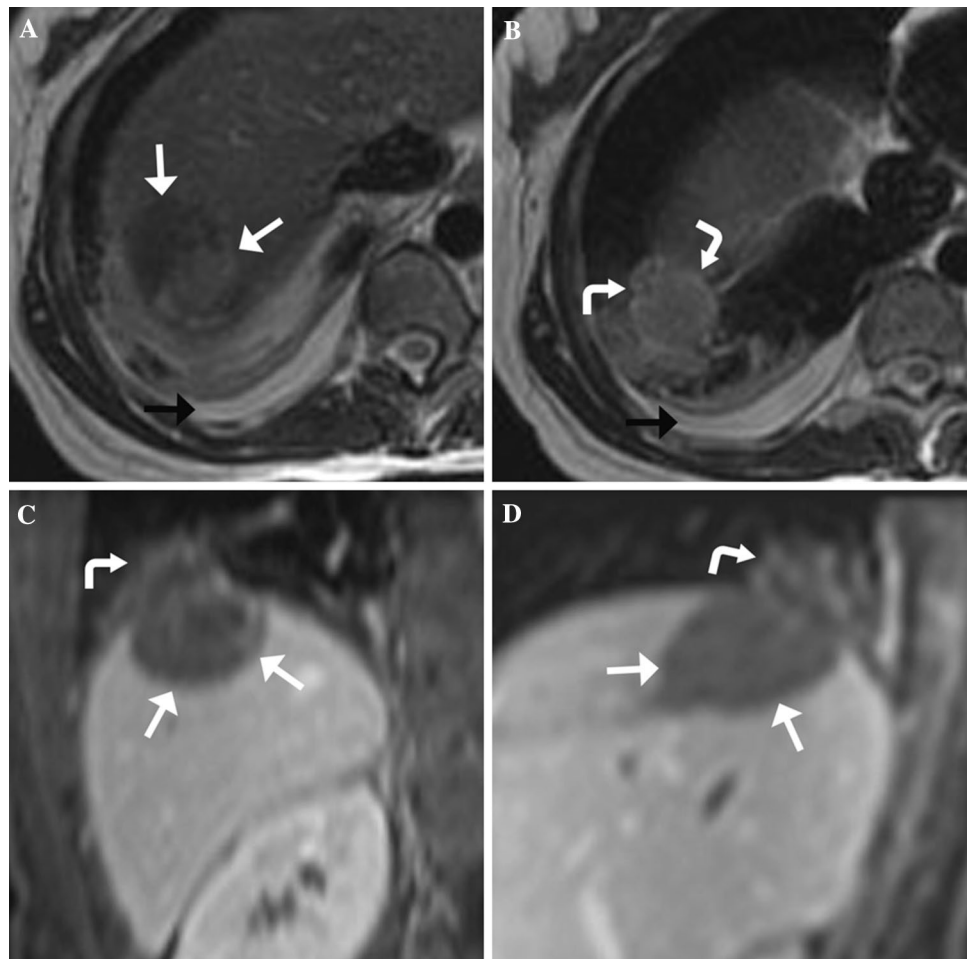
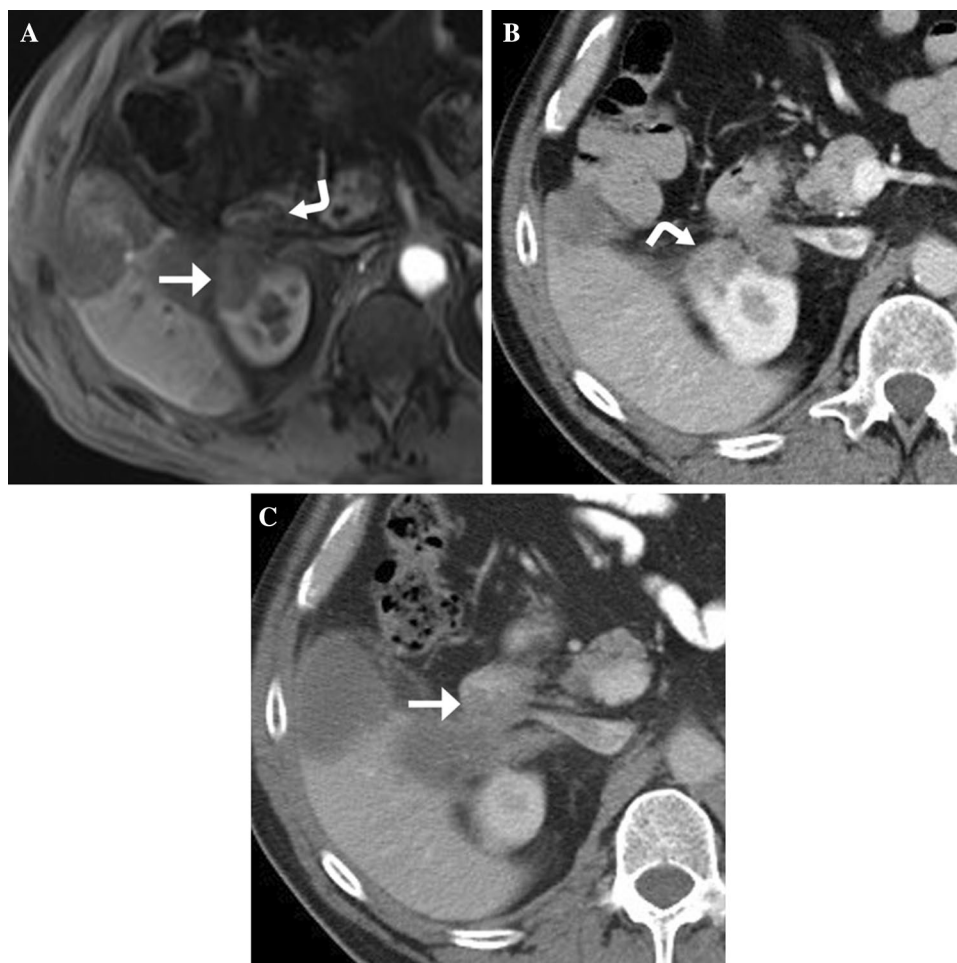


Fig. 25 Sixty-two-year-old female who underwent cryoablation of a gastrointestinal stromal tumor metastasis. **a** Axial, 24-h, post-procedure, T1-weighted, fat-saturated, contrast-enhanced MR image demonstrates non-target organ ablation of the adjacent kidney (arrow) and duodenum (curved arrow). **b** and **c** Axial CT images obtained 3 months after cryoablation demonstrates evolving non-target organ ablation zone that involves a portion of the kidney (curved arrow) and bowel wall (straight arrow)



who underwent radiofrequency ablation of hepatocellular carcinoma performed by Chang et al. [51], bilomas formed in 3.3% of patients. In the majority of patients, biloma formation is a minor complication of no clinical significance and resolve spontaneously [51]. However, occasionally bilomas can become symptomatic or infected requiring further treatment including percutaneous drainage [51, 73]. Bilomas appear as homogeneous T2 hyperintense, fluid signal areas in or adjacent to the ablation zone (Fig. 22d).

Non-target organ injury

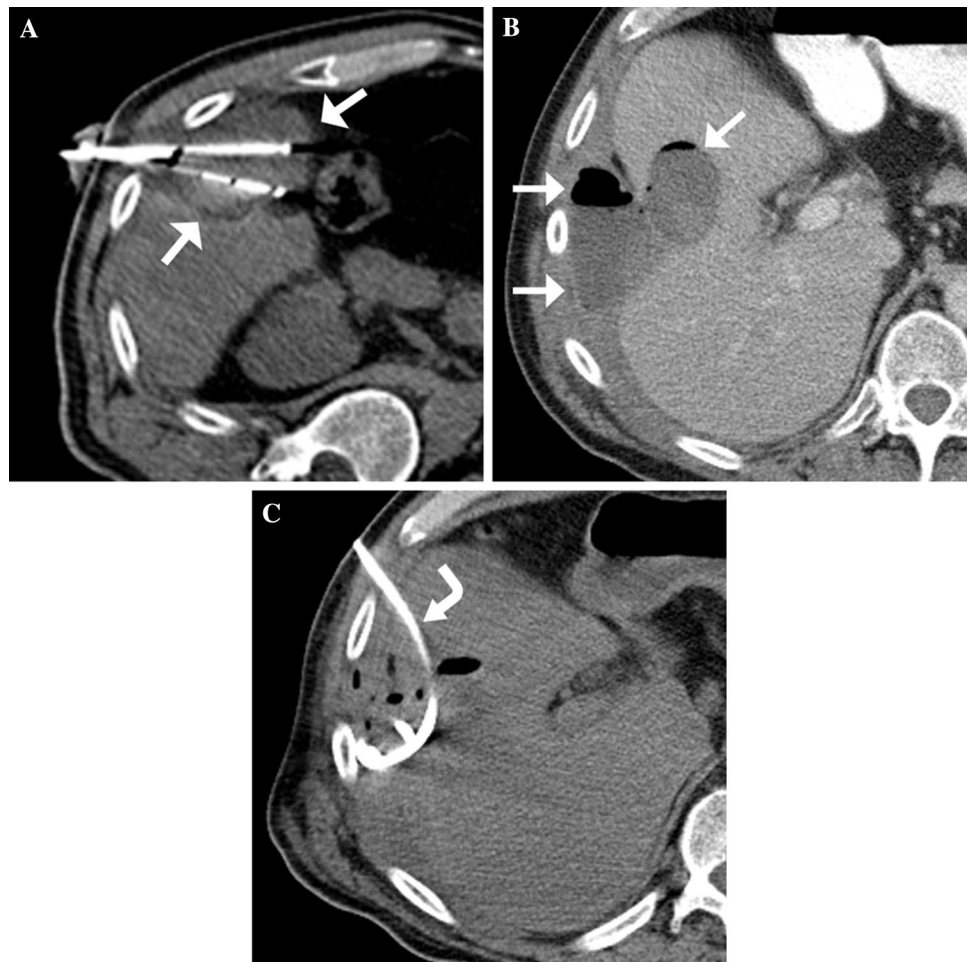
Pre-procedure planning enables strategies to avoid ablation injury of critical adjacent structures. Errors in planning, patient movement, and changes in heat-transfer effect may all affect the extent of the ablation zone. Small encroachments of the ablation zone into nearby spleen, kidney (Fig. 23), or lung (Fig. 24) are not likely to be clinically significant and in general do not complicate the cryoablation. However, it is advised that measures be taken to avoid non-target ablations

when possible. Ablation of bowel, major bile ducts or pancreas are important to avoid as injury to these structures can lead to significant morbidity and even mortality (Fig. 25) [74]. The gallbladder can be included in the ablation zone but it is essential that the peritoneal surface be avoided [53]. Other potential complications that may be detected on post-procedure imaging include pneumothorax and hemothorax [75, 76].

Infection

Although infrequent, intrahepatic abscess formation may occur with a reported rate of 0.3–1.7% after radiofrequency ablation [77]. Superinfection and subsequent abscess formation may occur after cryoablation, generally manifesting as an enlarging, hypodense or fluid-attenuation ablation zone on CT, or a markedly T2-hyperintense/T1-hypointense ablation zone on MRI. The presence of gas bubbles alone may be seen secondary to the ablation procedure, however if there are signs or symptoms of an infection, or if the gas

Fig. 26 Sixty-four-year-old male who underwent cryoablation of a colon cancer metastasis. **a** Axial, intra-procedural, unenhanced CT image shows cryoprobes and ablation zone (arrows) surrounding the target lesion. **b** and **c** Axial CT images obtained 4 months after cryoablation demonstrates collection of fluid and gas in the region of the ablation zone and in the peri-hepatic space (straight arrows) suggesting abscess. Percutaneous catheter drainage (curved arrow) yielded 110 cc of purulent fluid. Microbiology was positive for streptococcus anginosus



is accompanied by a fluid collection or peripheral enhancement, an abscess is likely (Fig. 26). Factors that can predispose to infection of the ablation zone include a history of biliary diversion including bilioenteric anastomosis, prior sphincterotomy, or biliary stents with small series reporting a rate of abscess complication as high as 44% after radiofrequency ablation [78]. Due to the high risk of septic complications, thermal ablation in a patient with a history of biliary diversion is a relative contraindication. If thermal ablation is performed in a patient with a history of biliary diversion, long-term post-procedural antibiotics can be considered as that has been shown to decrease risk of abscess formation [79].

Conclusion

A thorough understanding of the imaging findings associated with percutaneous hepatic tumor cryoablation helps distinguish those findings which are expected from those that

indicate the need for additional ablations to treat residual tumor or interventions to treat a complication.

References

1. Littrup PJ, Aoun HD, Adam B, Krycia M, Prus M, Shields A. Percutaneous cryoablation of hepatic tumors: long-term experience of a large U.S. series. *Abdom Radiol.* 2016 Apr;41(4):767–80.
2. Glazer DI, Tatli S, Shyn PB, Vangel MG, Tuncali K, Silverman SG. Percutaneous Image-Guided Cryoablation of Hepatic Tumors: Single-Center Experience With Intermediate to Long-Term Outcomes. *Am J Roentgenol.* 2017 Dec;209(6):1381–9.
3. Ross WB, Horton M, Bertolino P, Morris DL. Cryotherapy of Liver Tumours—A Practical Guide. *HPB Surgery.* 1995;8:7.
4. Shafir M, Shapiro R, Sung M, Warner R, Sicular A, Klipfeil A. Cryoablation of unresectable malignant liver tumors. *Am J Surg.* 1996;171(1):27–31.
5. Onik G, Porterfield B, Rubinsky B, Zemel R, Weaver L, Diamond D, et al. Ultrasound-guided hepatic cryosurgery in the treatment

- of metastatic colon carcinoma. Preliminary results. *Cancer*. 2006 Jun 29;67(4):901–7.
6. Weaver ML, Atkinson D, Zemel R. Hepatic cryosurgery in the treatment of unresectable metastases. *Surg Oncol*. 1995 Oct;4(5):231–6.
 7. Sarantou T, Bilchik A, Ramming KP. Complications of hepatic cryosurgery. *Semin Surg Oncol*. 1998 Dec 7;14(2):156–62.
 8. Lee FT, Littrup PJ, Chosy SG. Minimally invasive alternatives to traditional operative hepatic cryoablation: works in progress. *Surg Technol Int*. 1998;7:69–78.
 9. Shock SA, Laeseke PF, Sampson LA, Lewis WD, Winter III TC, Fine JP, et al. Hepatic Hemorrhage Caused by Percutaneous Tumor Ablation: Radiofrequency Ablation versus Cryoablation in a Porcine Model. *Radiology*. 2005 Jul;236(1):125–31.
 10. Dohi M, Harada J, Mogami T, Fukuda K, Toyama Y, Kashiwagi H. MR-guided percutaneous cryotherapy of malignant liver tumor under horizontal-magnetic open system: initial experience. *J Hepato-Biliary-Pancreatic Surg*. 2003 Oct 1;10(5):360–5.
 11. Morrison PR, Silverman SG, Tuncali K, Tatli S. MRI-guided cryotherapy. *J Magn Reson Imaging*. 2008 Feb;27(2):410–20.
 12. Bang HJ, Littrup PJ, Currier BP, Goodrich DJ, Aoun HD, Klein LC, et al. Percutaneous Cryoablation of Metastatic Lesions from Non-Small-Cell Lung Carcinoma: Initial Survival, Local Control, and Cost Observations. *J Vasc Interv Radiol*. 2012 Jun;23(6):761–9.
 13. Allen BC, Remer EM. Percutaneous Cryoablation of Renal Tumors: Patient Selection, Technique, and Postprocedural Imaging. *RadioGraphics*. 2010 Jul;30(4):887–900.
 14. Lee FT, Chosy SG, Littrup PJ, Warner TF, Kuhlman JE, Mahvi DM. CT-monitored percutaneous cryoablation in a pig liver model: pilot study. *Radiology*. 1999;211:687–92.
 15. Shyn PB, Mauri G, Alencar RO, Tatli S, Shah SH, Morrison PR, et al. Percutaneous imaging-guided cryoablation of liver tumors: predicting local progression on 24-hour MRI. *Am J Roentgenol*. 2014;203(2):W181–W191.
 16. Silverman SG, Tuncali K, Adams DF, vanSonnenberg E, Zou KH, Kacher DF, et al. MR imaging-guided percutaneous cryotherapy of liver tumors: initial experience. *Radiology*. 2000;217(3):657–664.
 17. Weiss J, Rempp H, Clasen S, Notohamiprodjo M, Keßler D-E, Pereira PL, et al. Diagnostic accuracy of different magnetic resonance imaging sequences for detecting local tumor progression after radiofrequency ablation of hepatic malignancies. *Eur J Radiol*. 2017 Sep;94:85–92.
 18. Hoffmann R, Rempp H, Schraml C, Schwenzer N, Grözinger G, Blumenstock G, et al. Diffusion-weighted imaging during MR-guided radiofrequency ablation of hepatic malignancies: analysis of immediate pre- and post-ablative diffusion characteristics. *Acta Radiol*. 2015 Aug;56(8):908–16.
 19. Shao et al. - 2017 - Evaluation of efficacy of transcatheter arterial c.pdf [Internet]. [cited 2019 Mar 6]. Available from: <https://www.ncbi.nlm.nih.gov/pmc/articles/PMC5279074/pdf/medi-96-e5518.pdf>
 20. García-Figueiras R, Goh VJ, Padhani AR, et al. (2013) CT Perfusion in Oncologic Imaging: a Useful Tool? *Am J Roentgenol*. 200(1):8–19
 21. d'Assignies G, Couvelard A, Bahrami S, Vullierme M-P, Hammel P, Hentic O, et al. Pancreatic Endocrine Tumors: Tumor Blood Flow Assessed with Perfusion CT Reflects Angiogenesis and Correlates with Prognostic Factors. *Radiology*. 2009 Feb;250(2):407–16.
 22. Goh V, Halligan S, Daley F, Wellsted DM, Guenther T, Bartram CI. Colorectal Tumor Vascularity: Quantitative Assessment with Multidetector CT—Do Tumor Perfusion Measurements Reflect Angiogenesis? *Radiology*. 2008 Nov;249(2):510–7.
 23. Erinjeri JP, Clark TWI. Cryoablation: Mechanism of Action and Devices. *J Vasc Interv Radiol*. 2010 Aug;21(8):S187–91.
 24. Popken F, Seifert JK, Engelmann R, Dutkowski P, Nassir F, Junginger T. Comparison of Iceball Diameter and Temperature Distribution Achieved with 3-mm Accuprobe Cryoprobes in Porcine and Human Liver Tissue and Human Colorectal Liver Metastases in Vitro. *Cryobiology*. 2000 Jun;40(4):302–10.
 25. Cheolkyun Kim, O'Rourke AP, Mahvi DM, Webster JG. Finite-Element Analysis of *Ex Vivo* and *In Vivo* Hepatic Cryoablation. *IEEE Trans Biomed Eng*. 2007;54(7):1177–85.
 26. Chosy SG, Nakada SY, Lee FT, Warner TF. Monitoring renal cryosurgery: predictors of tissue necrosis in swine. *J Urol*. 1998;159(4):1370–1374.
 27. Jacob G, Kurzer MN, Fuller BJ. An assessment of tumor cell viability after in vitro freezing. *Cryobiology*. 1985;22(5):417–426.
 28. Wu B, Xiao Y-Y, Zhang X, Zhang A-L, Li H-J, Gao D-F. Magnetic resonance imaging-guided percutaneous cryoablation of hepatocellular carcinoma in special regions. *Hepatobiliary Pancreat Int*. 2010;9(4):384–392.
 29. Zhang A, Xu LX, Sandison GA, Cheng S. Morphological study of endothelial cells during freezing. *Phys Med Biol*. 2006 Dec 7;51(23):6047–60.
 30. Weber SM, Lee FT, Chinn DO, Warner T, Chosy SG, Mahvi DM. Perivascular and intralesional tissue necrosis after hepatic cryoablation: results in a porcine model. *Surgery*. 1997;122(4):742–747.
 31. Baust JG, Gage AA, Clarke D, Baust JM, Buskirk RV. Cryosurgery—a putative approach to molecular-based optimization. *Cryobiology*. 2004 Apr;48(2):190–204.
 32. Baust JG, Gage AA. The molecular basis of cryosurgery. *BJU Int*. 2005 Jun;95(9):1187–91.
 33. Kuszyk BS, Choti MA, Urban BA, Chambers TP, Bluemke DA, Sitzmann JV, et al. Hepatic tumors treated by cryosurgery: normal CT appearance. *AJR Am J Roentgenol*. 1996;166(2):363–368.
 34. Tatsutani K, Rubinsky B, Onik G, Dahiya R. Effect of thermal variables on frozen human primary prostatic adenocarcinoma cells. *Urology*. 1996;48(3):441–447.
 35. Gage AA, Guest K, Montes M, Caruana JA, Whalen DA. Effect of varying freezing and thawing rates in experimental cryosurgery. *Cryobiology*. 1985;22(2):175–182.
 36. Kuszyk BS, Boitnott JK, Choti MA, Bluemke DA, Sheth S, Magee CA, et al. Local tumor recurrence following hepatic cryoablation: radiologic-histopathologic correlation in a rabbit model. *Radiology*. 2000;217(2):477–486.
 37. Permpongkosol S, Link RE, Kavoussi LR, Solomon SB. Temperature Measurements of the Low-Attenuation Radiographic Ice Ball During CT-Guided Renal Cryoablation. *Cardiovasc Intervent Radiol*. 2008 Jan;31(1):116–21.
 38. Rosenberg MD, Kim CY, Tsivian M, Suberlak MN, Sopko DR, Polascik TJ, et al. Percutaneous Cryoablation of Renal Lesions With Radiographic Ice Ball Involvement of the Renal Sinus: Analysis of Hemorrhagic and Collecting System Complications. *Am J Roentgenol*. 2011 Apr;196(4):935–9.
 39. Littrup PJ, Jallad B, Vorugu V, Littrup G, Currier B, George M, et al. Lethal Isotherms of Cryoablation in a Phantom Study: Effects of Heat Load, Probe Size, and Number. *J Vasc Interv Radiol*. 2009 Oct;20(10):1343–51.

40. Lu A, Daniel BL, Pauly JM, Butts Pauly K. Improved slice selection for R2* mapping during cryoablation with eddy current compensation. *J Magn Reson Imaging*. 2008 Jul;28(1):190–8.
41. Bhagavatula SK, Chick JFB, Chauhan NR, Shyn PB. Artificial ascites and pneumoperitoneum to facilitate thermal ablation of liver tumors: a pictorial essay. *Abdom Radiol*. 2017 Feb;42(2):620–30.
42. Farrell MA, Charboneau JW, Callstrom MR, Reading CC, Engen DE, Blute ML. Paraneoplastic water instillation: a technique to prevent bowel injury during percutaneous renal radiofrequency ablation. *Am J Roentgenol*. 2003;181(5):1315–1317.
43. Bodily KD, Atwell TD, Mandrekar JN, Farrell MA, Callstrom MR, Schmit GD, et al. Hydrodisplacement in the Percutaneous Cryoablation of 50 Renal Tumors. *Am J Roentgenol*. 2010 Mar;194(3):779–83.
44. Arellano RS, Garcia RG, Gervais DA, Mueller PR. Percutaneous CT-Guided Radiofrequency Ablation of Renal Cell Carcinoma: Efficacy of Organ Displacement by Injection of 5% Dextrose in Water Into the Retroperitoneum. *Am J Roentgenol*. 2009 Dec;193(6):1686–90.
45. Kierans AS, Elazzazi M, Braga L, Leonardou P, Gerber DA, Burke C, et al. Thermoablative Treatments for Malignant Liver Lesions: 10-Year Experience of MRI Appearances of Treatment Response. *Am J Roentgenol*. 2010 Feb;194(2):523–9.
46. Ahmed M, Solbiati L, Brace CL, Breen DJ, Callstrom MR, Charboneau JW, et al. Image-guided Tumor Ablation: Standardization of Terminology and Reporting Criteria—A 10-Year Update. *Radiology*. 2014 Oct;273(1):241–60.
47. Goldberg SN, Grassi CJ, Cardella JF, Charboneau JW, Dodd GD, Dupuy DE, et al. Image-guided Tumor Ablation: Standardization of Terminology and Reporting Criteria. *Radiology*. 2005 Jun;235(3):728–39.
48. Limanond P, Zimmerman P, Raman SS, Kadell BM, Lu DS. Interpretation of CT and MRI after radiofrequency ablation of hepatic malignancies. *Am J Roentgenol*. 2003;181(6):1635–1640.
49. Sainani NI, Silverman SG, Tuna IS, Aghayev A, Shyn PB, Tuncali K, et al. Incidence and clinical sequelae of portal and hepatic venous thrombosis following percutaneous cryoablation of liver tumors. *Abdom Radiol*. 2016 May;41(5):970–7.
50. Kim AY, Rhim H, Park M, Lee MW, Kim Y-S, Choi D, et al. Venous Thrombosis After Radiofrequency Ablation for Hepatocellular Carcinoma. *Am J Roentgenol*. 2011 Dec;197(6):1474–80.
51. Chang IS, Rhim H, Kim SH, Kim Y, Choi D, Park Y, et al. Biloma Formation After Radiofrequency Ablation of Hepatocellular Carcinoma: Incidence, Imaging Features, and Clinical Significance. *Am J Roentgenol*. 2010 Nov;195(5):1131–6.
52. Kim SH, Lim HK, Choi D, Lee WJ, Kim SH, Kim MJ, et al. Changes in bile ducts after radiofrequency ablation of hepatocellular carcinoma: frequency and clinical significance. *Am J Roentgenol*. 2004;183(6):1611–1617.
53. Fairchild AH, Tatli S, Dunne RM, Shyn PB, Tuncali K, Silverman SG. Percutaneous Cryoablation of Hepatic Tumors Adjacent to the Gallbladder: Assessment of Safety and Effectiveness. *J Vasc Interv Radiol*. 2014 Sep;25(9):1449–55.
54. Nair S, Silverman SG, Tuncali K, Obuchowski NA, vanSonnenberg E, Shankar S. Biochemical and hematologic alterations following percutaneous cryoablation of liver tumors: experience in 48 procedures. *Radiology*. 2008;16:90–5.
55. Sainani NI, Gervais DA, Mueller PR, Arellano RS. Imaging After Percutaneous Radiofrequency Ablation of Hepatic Tumors: Part 1, Normal Findings. *Am J Roentgenol*. 2013 Jan;200(1):184–93.
56. Tatli S, Acar M, Silverman S. Percutaneous cryoablation: techniques and clinical applications. *Diagn Interv Radiol [Internet]*. 2008 [cited 2018 Jan 7]; Available from: http://www.dirjournal.org/sayilar/29/buyuk/pdf_DIR_276.pdf
57. Wile GE, Leyendecker JR, Krehbiel KA, Dyer RB, Zagoria RJ. CT and MR Imaging after Imaging-guided Thermal Ablation of Renal Neoplasms. *RadioGraphics*. 2007 Mar;27(2):325–39.
58. Gage AA, Baust J. Mechanisms of Tissue Injury in Cryosurgery. *Cryobiology*. 1998 Nov;37(3):171–86.
59. Lim HK, Choi D, Lee WJ, Kim SH, Lee SJ, Jang H-J, et al. Hepatocellular Carcinoma Treated with Percutaneous Radio-frequency Ablation: Evaluation with Follow-up Multiphase Helical CT. *Radiology*. 2001 Nov;221(2):447–54.
60. Okusaka T, Okada S, Ueno H, Ikeda M, Shimada K, Yamamoto J, et al. Satellite lesions in patients with small hepatocellular carcinoma with reference to clinicopathologic features. *Cancer*. 2002 Nov 1;95(9):1931–7.
61. Brilllet P-Y, Paradis V, Brancatelli G, Rangheard A-S, Consigny Y, Plessier A, et al. Percutaneous Radiofrequency Ablation for Hepatocellular Carcinoma Before Liver Transplantation: A Prospective Study with Histopathologic Comparison. *Am J Roentgenol*. 2006 May;186(5_supplement):S296–305.
62. Dromain C, de Baere T, Elias D, Kuoch V, Ducreux M, Boige V, et al. Hepatic Tumors Treated with Percutaneous Radio-frequency Ablation: CT and MR Imaging Follow-up. *Radiology*. 2002 Apr;223(1):255–62.
63. Tatli S, Acar M, Tuncali K, Sadow CA, Morrison PR, Silverman SG. MRI assessment of percutaneous ablation of liver tumors: Value of subtraction images. *J Magn Reson Imaging*. 2013 Feb;37(2):407–13.
64. Purandare NC, Rangarajan V, Shah SA, Sharma AR, Kulkarni SS, Kulkarni AV, et al. Therapeutic Response to Radiofrequency Ablation of Neoplastic Lesions: FDG PET/CT Findings. *RadioGraphics*. 2011 Jan;31(1):201–13.
65. Shyn PB, Oliva MR, Shah SH, Tatli S, Catalano PJ, Silverman SG. MRI contrast enhancement of malignant liver tumours following successful cryoablation. *Eur Radiol*. 2012 Feb;22(2):398–403.
66. Jaskolka JD, Asch MR, Kachura JR, Ho CS, Ossip M, Wong F, et al. Needle Tract Seeding after Radiofrequency Ablation of Hepatic Tumors. *J Vasc Interv Radiol*. 2005 Apr;16(4):485–91.
67. Llovet JM, Vilana R, Brú C, Bianchi L, Salmeron JM, Boix L, et al. Increased risk of tumor seeding after percutaneous radiofrequency ablation for single hepatocellular carcinoma. *Hepatology*. 2003 Dec 30;33(5):1124–9.
68. Livraghi T, Solbiati L, Meloni MF, Gazelle GS, Halpern EF, Goldberg SN. Treatment of Focal Liver Tumors with Percutaneous Radio-frequency Ablation: Complications Encountered in a Multicenter Study. *Radiology*. 2003 Feb;226(2):441–51.
69. Gervais DA, Arellano RS. Percutaneous Tumor Ablation for Hepatocellular Carcinoma. *Am J Roentgenol*. 2011 Oct;197(4):789–94.
70. Sainani NI, Gervais DA, Mueller PR, Arellano RS. Imaging After Percutaneous Radiofrequency Ablation of Hepatic Tumors: Part 2, Abnormal Findings. *Am J Roentgenol*. 2013 Jan;200(1):194–204.
71. Lokken RP, Gervais DA, Arellano RS, Tuncali K, Morrison PR, Tatli S, et al. Inflammatory Nodules Mimic Applicator Track Seeding After Percutaneous Ablation of Renal Tumors. *Am J Roentgenol*. 2007 Oct;189(4):845–8.
72. Francica G, Marone G, Solbiati L, D'Angelo V, Siani A. Hemobilia, intrahepatic hematoma and acute thrombosis with cavernomatous transformation of the portal vein after percutaneous thermoablation of a liver metastasis. *Eur Radiol*. 2000;10(6):926–929.
73. Shankar S, vanSonnenberg E, Silverman SG, Tuncali K, Morrison PR. Diagnosis and treatment of intrahepatic biloma complicating radiofrequency ablation of hepatic metastases. *Am J Roentgenol*. 2003;181(2):475–477.
74. Georgiades CS, Hong K, Bizzell C, Geschwind J-F, Rodriguez R. Safety and Efficacy of CT-guided Percutaneous Cryoablation for Renal Cell Carcinoma. *J Vasc Interv Radiol*. 2008 Sep;19(9):1302–10.

75. Akahane M, Koga H, Kato N, Yamada H, Uozumi K, Tateishi R, et al. Complications of Percutaneous Radiofrequency Ablation for Hepato-cellular Carcinoma: Imaging Spectrum and Management. *RadioGraphics*. 2005;25(suppl_1):S57–68.
76. Dunne RM, Shyn PB, Sung JC, Tatli S, Morrison PR, Catalano PJ, et al. Percutaneous treatment of hepatocellular carcinoma in patients with cirrhosis: A comparison of the safety of cryoablation and radiofrequency ablation. *Eur J Radiol*. 2014 Apr;83(4):632–8.
77. Choi D, Lim HK, Kim MJ, Kim SJ, Kim SH, Lee WJ, et al. Liver abscess after percutaneous radiofrequency ablation for hepatocellular carcinomas: frequency and risk factors. *Am J Roentgenol*. 2005;184(6):1860–1867.
78. Elias D, Di Pietroantonio D, Gachot B, Menegon P, Hakime A, de Baere T. Liver abscess after radiofrequency ablation of tumors in patients with a biliary tract procedure. *Gastroenterologie Clin Biol*. 2006;30:823–7.
79. Welch BT, Schmitz JJ, Atwell TD, McGauvran AM, Kurup AN, Callstrom MR, et al. Evaluation of infectious complications following percutaneous liver ablation in patients with bilioenteric anastomoses. *Abdom Radiol*. 2017 May;42(5):1579–82.

Publisher's Note Springer Nature remains neutral with regard to jurisdictional claims in published maps and institutional affiliations.